SYNTHESIS OF NANO LEAD OXIDE FOR THE APPLICATION OF LEAD-ACID ENERGY STORAGE DEVICES

WONG KIN NYAP

MASTER OF PHILOSOPHY (MPHIL)
CHEMICAL AND ENVIRONMENTAL ENGINEERING

FACULTY OF ENGINEERING
UNIVERSITY OF NOTTINGHAM MALAYSIA CAMPUS (UNMC)

2017

ACKNOWLEDGEMENT

First of all, I would like to express my deepest gratitude to my supervisor, Prof. Khiew Poi Sim, and research colleague, Dr. Chiu Wei Siong for constructive guidance in succeeding this essential research. Moreover, my appreciation is also extended to Yokohama Battery (M) Sdn. Bhd. for the sponsorship of tuition fees throughout my entire research tenure with University of Nottingham Malaysia Campus. Besides that, I am also grateful with additional research funds provided by my supervisor's team in purchasing all necessary experimental tools to ensure the project is completed to our expectation.

CONTENTS

Abstract

Over the past decades, efforts have been emphasized on electric vehicles (EV) as a major solution to reduce carbon emission for greener environment. While one of the core design components of EV is the energy storage device which is to ensure sustainable power supply in the drive train system. However, existing energy storage applied in EV is relatively expensive, so, affordable and feasible energy storage needs to be explored to achieve the objective of fuel economy.

As a matter of fact, technology of lead-acid battery has been around for more than a century, the established manufacturing and recycling processes, as well as overall simplistic product designs with relatively high power and energy densities, are attracting global researchers to harness their ultimate innovation. This is done via the essence of nanotechnology in transforming existing product design of lead-acid battery so that it is applicable in EV power train. Despite the challenges are inevitable, global researchers accept that electrode material with novel microstructural is the key solution to the problem.

Recently, nanodendritic PbO_2 has been the attractive material with unique morphology and enhanced electrochemical performance for lead-acid electrochemical storage devices. Thus far, many studies have only been investigated this unique material via electrodeposition technique. In this study, flower-like PbO consisting of three

dimensional nanoflakes was synthesized and used as a starting precursor to form nanodendritic PbO_2 via an electrochemical oxidation at constant voltage in the presence of electrolyte.

According to the XRD results, the as-synthesized PbO was perfectly indexed to the diffraction peaks of pure PbO with a mixture of orthorhombic and tetragonal structures. The same is true for PbO_2 which was electrochemically oxidized from the as-synthesized PbO. Meanwhile, both SEM results show that the as-synthesized PbO was characterized with flower-like structures providing high active surface area to form nanodendritic PbO_2 via electrochemical oxidation at constant voltage based on periodic bond chain theory. The formed nanodendritic PbO_2 delivered a first discharge capacity of 170 $mAhg^{-1}$ at 200 mAg^{-1} and displayed improved cyclic voltammetry curve. This suggested that the formation of nanodendrites on the primary surface of agglomerated PbO_2 provides larger crystallite network structures for better material utilization at high discharge rate.

Upon the completion of current experimental work, a few general conclusions of this work have unfolded other research which focus on fabricating a prototype of lead-acid hybrid supercapacitor for evaluation.

List of Abbreviations

BSE	-	Backscattering Electron
C20	-	Capacity Ampere-Hour Rating at 20 hours
Ca	-	Calcium
CCA	-	Cold Cranking Ampere
Cp	-	Heat Capacity
CV	-	Cyclic Voltammetry
E^o	-	Standard Electrode Potential
EV	-	Electrical Vehicle
HEV	-	Hybrid Electrical Vehicle
Hg	-	Mercury
HRPSoC	-	High Rate Partial State of Charge
H_2SO_4	-	Sulfuric Acid
ICE	-	Internal Combustion Engine
K_2SO_4	-	Potassium Sulfate
LAESD	-	Lead-Acid Energy Storage Device

NaOH	-	Sodium Hydroxide
PAM	-	Positive Active Material
Pb	-	Lead
$PbBr_2$	-	Lead Bromide
PBC	-	Periodic Bond Chain
$PbCO_3$	-	Lead Carbonate
PbO	-	Lead Monoxide
PbO_2	-	Lead Dioxide
$PbSO_4$	-	Lead Sulfate
$Pb(OH)_2$	-	Lead Hydroxide
$Pb(NO_3)_2$	-	Lead Nitrate
Pb_2O_3	-	Lead Trioxide
Pb_3O_4	-	Red Lead
S^o	-	Standard Entropy
Sb	-	Antimony
SE	-	Secondary Electron
SEM	-	Scanning Electron Microscopy

SLI	-	Starting Lighting Ignition
SOC	-	State of Charge
Sn	-	Tin
SPT	-	Spray Pyrolysis Technique
V^o	-	Standard Cell Voltage
XRD	-	X-ray Powder Diffraction
ΔG_f^o	-	Standard Free Energy of Formation
ΔH_f^o	-	Enthalpy of Formation
3BS	-	Tribasic Lead Sulfate
4BS	-	Tetrabasic Lead Sulfate

List of Figures

List of Tables

Chapter 1

1.0 Introduction

Lead-acid battery is a secondary rechargeable battery comprising a series of galvanic cells that transforms chemical energy into electrical energy for a variety of applications such as industrial stationary power source, automotive vehicles, electrical vehicles (EVs), hybrid electric vehicles (HEVs) and communication equipments, each with its own distinctive duty cycle [1].

As prominent application of lead-acid battery prevails in conventional automotive vehicles, its technical function is literally similar to other application mentioned but at a different scale of electrical power required, which, in internal-combustion-engine (ICE) vehicles, the battery provides a quick pulse of high current for starting and a lower, sustained current for other purposes; the battery remains at a high state-of-charge (SOC) for most of the time. The same is true for batteries used for electrical vehicles which are expected to undergo deep discharges and recharges over periods of a few hours repeatedly (so-called 'deep-discharge duty'). On the other hand, in between the extreme cases of float duty and deep discharge, the batteries in HEVs spend most of the time cycling about an intermediate SOC, often near 50% (so-called 'partial-state-of-discharge duty'). Thus, in all cases, the battery must be able to provide adequate power for the task in hand. However, this may be a higher requirement for batteries in EVs and

HEVs than for batteries in ICE vehicles, which is also known as starting-lighting-ignition (SLI) batteries [2].

As the technological and market trends of EVs and HEVs grow along the recent years as part of the critical efforts to mitigate the worsening condition of global climate change by lowering fuel consumption for lesser carbon gas emission, the power requirement of these technologies are proportionally increasing as well. When the first prototype model of HEV was invented in R&D lab of Honda Co. Ltd. in 2001, the power train system of the electrical automobile was set to undergo a major change [3]. The lead-acid battery community anticipated a serious challenge in 2007 as its largest market for SLI batteries would be substantially replaced by EVs or HEVs batteries with a markedly higher electrical power requirement. The crux of the challenge at that time was that neither the conventional SLI batteries nor deep-cycle lead-acid batteries were able to perform successfully in the high-rate partial-state-of-charge (HRPSoC) duty which is required by the new electrical automobile systems [4].

Despite the fact that the main challenges of transforming conventional lead-acid batteries to meet energy and power requirements of future automobiles are getting more excruciating, motivation and research efforts have never been abandoned before to continuously explore invention on lead-acid technology with low cost manufacturing cost, simplicity in design, reliability, recyclability and relatively high safety [5]. All these

features are the primary driving force to harness the lead-acid battery of next generation that would improve fuel economy at an acceptable cost.

Along the years of optimization numerous researches on the battery performance, main technical challenges have been identified which are the continuity of supply, contact and interaction of reactants with electrode materials and electrolyte. In principal, this requires an adequate supply of acid, active material of high surface area, good contact between the particles of the active material (particularly in positive plates that show a tendency to expand during charge-discharge service cycle), and the minimization of the insulating effects of $PbSO_4$. Most importantly, the limitation of this battery is caused by the underlying reaction taking place between positive and negative electrodes via the so-called 'dissolution-precipitation mechanism' that inhibits rapid electron transfer. Consequently, this limitation is the critical reason that lead-acid battery fails prematurely in HRPSoC regimen of HEV duty [2].

Thus, in order to improve and alleviate the underlying limitation of lead-acid battery, novel, innovative and flexible cell designs to tackle specific application are no longer an option. Those elements are compulsory in research development especially in the rising trend of nanotechnology for producing electrode material with high active surface area and efficiency. Between 2005-2010, arduous researches in developing new lead-acid batteries by incorporating new electrode materials for HEV duty had finally paid off with a few successful inventions such as UltrabatteryTM, Lead-Carbon and Thin Metal Foil

batteries. These batteries have passed the requirement of HEV duty where the negative electrode material was partially replaced by carbon with high surface area like activated carbon or graphite [7].

Remarkably, the successful emergence of new generation of lead-acid batteries has proven that innovative modifications to traditional lead-acid battery enable a low-cost route to improve respective vehicle performance. However, the journey is still far from achieving fully operational battery storage in full EV. Hence, with the growing research interest in nanotechnology, invention of lead-carbon based batteries, and the rise of supercapacitor have sparked an innovative research idea among researchers around the globe with lead to the development of prototype of lead-acid energy storage device (LAESD). This is lead-acid hybrid supercapacitor, which is considered as a suitable candidate to provide sufficient rapid power to all EVs at an acceptable cost.

Technically, lead-acid hybrid supercapacitor consists of PbO_2 nanoparticles and activated carbon used as positive and negative electrode materials respectively in a spiral cell design to replenish the drawback of lead-acid batteries [6, 7]. Henceforth, the successful emergence of new generation of LAESD has been part of the continuous driving force in developing and fabricating novel electrode materials with excellent electrochemical properties. As nanotechnology has become essentially significant, many researchers around the world have turned their focus on synthesizing nanostructured particles as electrode materials of LAESD with various morphologies,

crystallite sizes and shapes, which are widely accepted as important characteristics to influence the final electrochemical performance of LAESD [8].

Thus, a number of extensive reports showed the synthesis of various nanostructured PbO with respect to its electrochemical performance, where PbO was the very first precursor being used to prepare active material for LAESD especially in producing commercial lead-acid battery. Throughout the years, nanostructured PbO has been synthesized via spray pyrolysis [9], chemical solution method [10], hydrothermal method [11], sonochemical [12], and electrochemical deposition [13] to enhance the discharge capacity, charge acceptance and operating life of lead-acid battery.

Nanostructured PbO_2 has also been extensively studied in its final form of positive active material for LAESD. The investigation on how influential the microstructural parameters of PbO_2 contributing to the electrochemical performance is rather difficult, as there are too many factors associated with the preparation of pasted plate electrodes prior to the formation of PbO_2. Therefore, many studies have focused on the electrodeposition of unique microstructures and sizes of PbO_2 which allow essential microstructural parameters to be identified in line with the improved electrochemical property [14].

Recently, there has been a rising interest in synthesizing three-dimensional dendritic nanostructures of PbO_2 as the electrode material in LAESD, which has been proven to show enhanced electrochemical performance via electrodeposition technique. The dendritic nanostructure is significantly larger in surface area for high charge and mass transports attributed to its well-connected structure [15]. However, there are only few reports showing the synthesis and electrochemical property of nanodendritic PbO_2. Thus far, there has never been a report indicating the desired material is prepared via electrochemical oxidation of active paste (basic lead sulfate) which is produced by using the starting precursor of PbO.

In order to know how starting precursor influences the electrochemical property of PbO_2 as positive electrode and sponge Pb as negative electrode, investigation in this area is necessary to be explored further in nano-scale. This uncharted territory has been around for decades despite the fact that the existing manufacturing process has been using the so-called ‘formation process’ which is similar to the electrochemical oxidation or reduction on the starting precursors to acquire respective final electrode materials for battery to function properly. Unlike electrodeposition, this area of study is readily implementable in the established production process of lead-acid battery or other LAESD processes to obtain the desired microstructures with enhanced electrochemical performance at an economical cost.

Therefore, prior to propose a constructive method in synthesizing PbO with interesting morphology leading to desired PbO_2 with unique microstructure and performance, properties of PbO such as material microstructure, polymorphism and its synthesis methods are explored as well as reviewing the state-of-the-art researches on how electrochemical properties of PbO_2 were influenced by this starting precursor.

1.1 Motivation of the project

Over the years, the major challenge in designing a performing energy storage device for HEV or EV technology remains the same, which is to achieve an economic cost at comparative energy efficiency for the desired application as part of the efforts to mitigate the worsening condition of greenhouse gas, environment pollution, climate change and depletion of fossil fuels [16, 17].

Among these energy storage devices, undoubtedly, LAESD such as lead-acid battery and lead-acid hybrid supercapacitor are being considered as the suitable candidates to fulfill that purpose in EV technology as those are cost efficient, relatively high specific energy and power efficiencies, reliable safety and furthermore, it is readily recyclable for better control of environmental pollution as mentioned in the introduction section.

Although nanotechnology has been the prevailing field in synthesizing nanoparticles for lead-acid hybrid supercapacitor, the developments in reducing cost of innovative

synthetic approach and scalable production capacity of the efficient nanomaterials are still in a stage of infancy if compared to the established commercial battery making of lead oxide such as Shimadzu ball mill, Hardinge cone ball mill, and Barton-pot [18].

Moreover, most of the innovative approaches are independent of the existing production process of making LAESD where production machines and delicate control measures with new engineering designs are necessary which indirectly increases the cost of production.

In addition to delicate engineering design and scalable production capacity, the organic solvents and surfactants used in synthetic approaches are also expensive which will be discussed further in later section. Thus, while maintaining green environmental synthetic approach at lower cost and achieving higher production yield, investigation needs to be carried out by making use of the existing technology to acquire the desired material with excellent electrochemical property.

1.2 Objective of the study

One of the objectives of this study is to synthesize PbO by using chemical solution without addition of surfactant to be used as template for the novel formation of PbO_2 via electrochemical oxidation at constant voltage in the presence of electrolyte, which serves as a potential precursor for fabricating 12V automotive lead-acid batteries.

Besides that, characterization of both nanodendritic PbO_2 and nanostructured PbO in terms of microstructure and electrochemical properties are also evaluated.

1.3 Scope of this project

Hence, addressing the shortcomings of existing synthetic approaches and utilizing the existing production process to acquire the desired material as starting precursor are necessary in this project which attempts to bridge the gap between scalable productions of PbO with the use of cheaper solvent.

As a result, preliminary investigation of this project will focus on the synthesis of PbO as starting precursor via one-pot chemical synthesis method in the absence of any structure director additive under vigorous stirring condition at room temperature. The as-synthesized PbO is dried in an oven and used as starting material to form active paste by mixing it with small amount of DI water and dilute sulfuric acid. The pasted and dried active paste is then electrochemically oxidized in sulfuric acid to form PbO_2 with enhanced electrochemical performance. The as-synthesized PbO and PbO_2 will be characterized by using an X-ray diffractometer X'PERT PRO PW3040 (Cu Kα radiation and wavelength, $\lambda = 0.154$ nm) for product quality and SEM (FEI Quanta-400 FESEM) for microstructural analysis, as well as potentiostat, Autolab PGSTAT302N in a classical three-electrode cell containing 4.7 M H_2SO_4 for electrochemical properties.

The results of this experiment will be analyzed for unraveling further potential experiments ahead to acquire the desired electrochemical material with respect to the application mentioned.

Chapter 2

2.0 Literature Review

2.1 Lead-acid Battery

The fundamental elements of the lead-acid battery were set in place over 150 years ago. Gaston Plante' [1] was the first to report that a useful discharge current could be drawn from a pair of lead plates that had been immersed in sulfuric acid and subjected to a charging current. Later, Camille Faure' [2] proposed the concept of the pasted plate. In the subsequent hundred years or so, the principal elements of the battery have not undergone any further radical change. The most commonly employed design has 'flat plates'. These are prepared by coating pastes of lead oxides and sulfuric acid on to conductive lead or lead-alloy 'grids', which act as current collectors. The plates are then electrolytically formed into 'active' materials.

In general, the current collector used in most conventional lead-acid batteries is a thick grid of lead (Pb) or its alloys with tin (Sn), calcium (Ca), or antimony (Sb). These grids are coated with positive or negative paste materials of basic lead sulfate which is produced by mixing lead oxide (PbO) as a starting precursor with sulfuric acid (H_2SO_4) and together with the respective additives such as security flock, carbon black, barium sulfate, vanisperse and etc. as negative plate. Likewise, security flock, red lead, and etc.

are used in positive plate. The pasted plates are later assembled into a cell and six cells are connected in series per battery. Each cell will be electrochemically formed in the presence of H_2SO_4 as electrolyte to complete a 2V cell, where the positive electrode in the cell will be electrochemically oxidized to become lead dioxide (PbO_2) while negative will be reduced to sponge Pb [1]. After the formation process, six cells in series will make a 12V lead-acid battery, which the fundamental was set since 100 years ago. The reason for PbO used as the template to form PbO_2 was due to the beauty of the conventional lead-acid battery where the process of electrochemical oxidation was developed to form the positive plate into PbO_2, while Pb in the negative plate. This combination of positive and negative plates generates a potential difference of 2V in the presence of electrolyte.

One alternative cell design uses positive plates in which the active material is contained in tubes, each fitted with a coaxial current-collector. Such ‘tubular plates’ serve to prevent shedding of the material during battery service. A more recent cell design, aimed at high-power applications, has a single pair of positive and negative plates which are interleaved with microfibre-glass mat separators and wound together in a cylindrical can (the ‘spirally wound’ or ‘jellyroll’ design). Ironically, this arrangement mimics that invented originally by Plante’ as mentioned. Schematics of the various plate types are given in Figure 2.1.

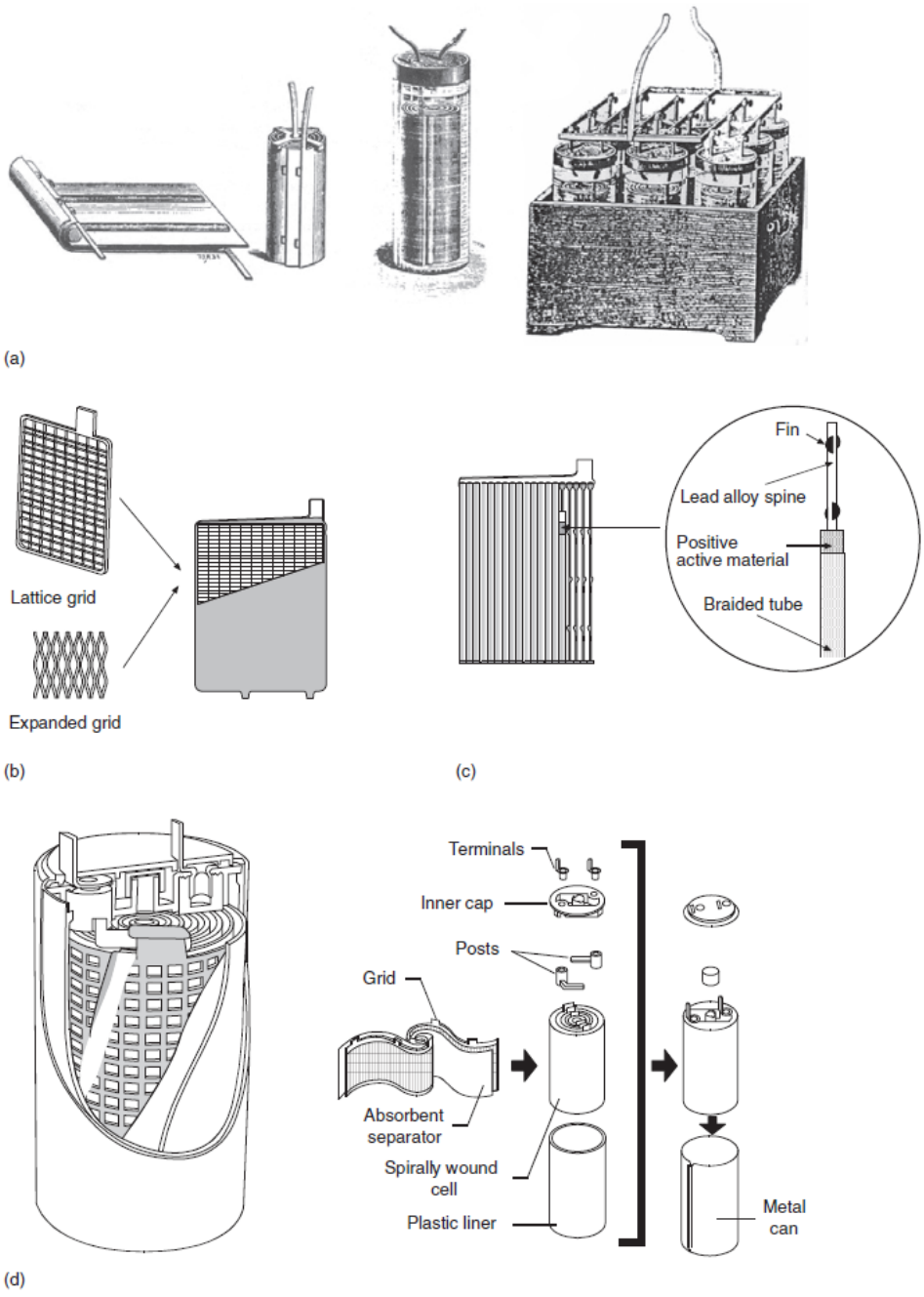

Figure 2.1: (a) Gaston Plante' cell and battery; (b) Flat plate; (c) tubular positive plate; and (d) Spiral-wound cell [2].

As discussed before, lead-acid battery has undergone many developments since its invention, most of which have involved modifications to the materials or design, rather than to the underlying chemistry. In all cases, PbO_2 serves as the positive active material, while Pb as the negative active material and H_2SO_4 as the electrolyte. The PbO_2 is present in two crystallite forms, namely, α-PbO_2 (orthorhombic) and β-PbO_2 (tetragonal); the latter is the predominant phase but there is some evidence to suggest that the relative abundances of the two polymorphs influence battery performance. More information about these polymorphs is elaborated in Section 2.3.5.

The electrode reactions of the cell are unusual in that the electrolyte is also one of the reactants as seen in the following equations for discharge and charge:

At the positive electrode:

$PbO_2 + 3H^+ + HSO_4^- + 2e^- \rightarrow PbSO_4 + 2H_2O$ (Discharge) - Equation 2.1

$PbO_2 + 3H^+ + HSO_4^- + 2e^- \leftarrow PbSO_4 + 2H_2O$ (Charge) - Equation 2.2

$E^o = +1.690$ V

At the negative electrode:

$Pb + HSO_4^- \rightarrow PbSO_4 + H^+ + 2e^-$ (Discharge) - Equation 2.3

$Pb + HSO_4^- \leftarrow PbSO_4 + H^+ + 2e^-$ (Charge) - Equation 2.4

$E^o = -0.358$ V

Where E^o is the standard electrode potential for each reaction, for example, the reaction is in a standard state. The overall cell reaction is:

$PbO_2 + Pb + 2H_2SO_4 \leftrightarrow 2PbSO_4 + 2H_2O$ ($V^o = +2.048$ V) - Equation 2.5

Where V^o is the standard cell voltage. It is noteworthy that this voltage is the highest for any type of commercial battery that employs an aqueous electrolyte solution. The processes taking place during charge-discharge of a lead-acid cell are displayed in Figure 2.2.

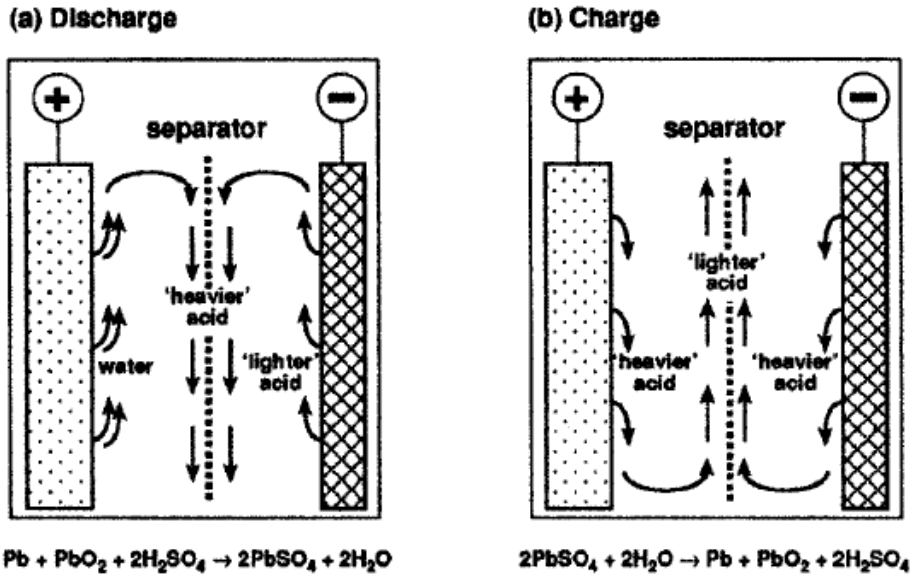

Figure 2.2: Schematic representation of processes taking place during charge-discharge of a lead-acid cell [1].

A key success in maximizing battery performance is to synthesize active material with high surface area. Thus, the synthesis of PbO nanoparticles as the starting precursor to form nano PbO_2 is necessary for lead-acid battery with distinguished performance.

2.2 Lead monoxide (PbO)

2.2.1 General application

PbO has wide commercial applications. In addition to the application in LAESD, it is also used in optical and electrical glasses; in vitreous enamels, glazes, and fine tableware; in lead soaps for varnishes; as a vulcanizing agent for rubber and plastics; and as a lubricant at high temperatures [18]. An important application of this oxide involves its use as the starting material for producing various lead pigments as well as other compounds of commercial interest such as lead arsenate, lead acetate, and sodium plumbite. Also, PbO is used in certain organic syntheses as a neutralizing agent.

2.2.2 Physical properties

PbO with a molecular weight of 223.30 g/mol exhibits two crystalline modifications, the reddish or orange-red alpha form, known as litharge, and the yellow beta form, massicot [19]. The alpha form constitutes tetragonal crystals while the beta modification is a yellow amorphous powder of orthorhombic crystal structure. The alpha form is stable at ordinary temperatures, converting to the beta form when heated at 489°C; density 9.35 g/cm^3 (beta form); Moh's hardness 2 (alpha form); the oxide melts at 888°C; vaporizes at 1,472°C with decomposition; vapor pressure 1 torr at 943°C and 5 torr at 1,039°C; practically insoluble in water (the solubility of alpha form is 17 mg/L at 20°C and that of beta form 23 mg/L at 22°C); insoluble in ethanol; soluble in dilute nitric acid and alkalies. Meanwhile, summary of the crystal structures of polymorphs is shown in Table 2.1.

Table 2.1: The crystal structure of PbO [19].

System	Characteristics	Essential Symmetry	Axes in unit cell	Angles in unit cell
Tetragonal (α-PbO)	Two equal axes and one unequal axis mutually perpendicular	One 4-fold axis	$a = b \neq c$	$\alpha = \beta = \gamma = 90^o$
Orthorhombic (β-PbO)	Three unequal-axes mutually perpendicular	Three mutually perpendicular 2-fold axes, or two planes intersecting in a 2-fold axis	$a \neq b \neq c$	$\alpha = \beta = \gamma = 90^o$

2.2.3 Thermochemical properties

The thermochemical properties of PbO are indicated in Table 2.2 below.

Table 2.2: Thermochemical properties of PbO [19].

Thermochemical Properties	Crystalline Phase	Energy
ΔH_f^o	Alpha form	-52.34 kcal/mol
ΔH_f^o	Beta form	-51.94 kcal/mol
ΔG_f^o	Alpha form	-45.15 kcal/mol
ΔG_f^o	Beta form	-44.91 kcal/mol
S^o	Alpha form	15.89 Cal/degree mol
S^o	Beta form	16.42 Cal/degree mol
C_p	Both forms	10.95 Cal/degree mol

Alpha form of PbO is higher than beta form in terms of enthalpy of formation and standard free energy of formation, while slightly lower than beta form with respect to standard entropy.

2.2.4 Commercial production of PbO

PbO is produced commercially via two common processes, Barton process and the Ball Mill process. The Ball-Mill process involves a reaction of molten lead with oxygen or air. In the Barton process, atomized molten lead is stirred in a mechanical furnace above 550 °C [18]. The molten metal splashed by a stirring paddle comes in contact with air and gets fed into the cover of the furnace through a pipe, thus forming a mist of finely dispersed lead monoxide. The mist also contains a small amount of unreacted lead. The mist is passed through an upright shaft where a major portion of unreacted lead falls back into the furnace. It is then rapidly cooled and collected in condensing chambers.

The crude product may contain 1 to 3% lead. It is finely ground and sold. The remaining lead in the crude product may be converted into lead monoxide by stirring the molten mass in the presence of air for several hours. The hot product is then cooled rapidly below 300°C to prevent any formation of lead tetroxide, Pb_3O_4. In an alternate process, a variation of the above method, molten lead is atomized in a shaft furnace [18]. An air stream carries the very finely divided metal into the hot zone of the shaft furnace where the metal evaporates and oxidizes producing very fine lead monoxide. The product is passed through the cold zone of the furnace and cooled rapidly. The product obtained is a yellow powder, the beta form of lead oxide, massicot, consisting of orthorhombic crystals. On the other hand, the red lead oxide (the tetragonal alpha modification) is obtained by slow cooling of the molten lead monoxide.

PbO is also produced by a modified Ball Mill process in which high purity lead balls placed in the mill are partially oxidized to produce black or grey oxide [19]. Both the red and yellow forms of oxide may be prepared via alkaline dehydration of lead hydroxide, $Pb(OH)_2$. An example of the Ball Mill process is illustrated in the Figure 2.3.

However, the PbO produced via Ball Mill and Barton Pot processes is low in surface area if compared to that synthesized by chemical method.

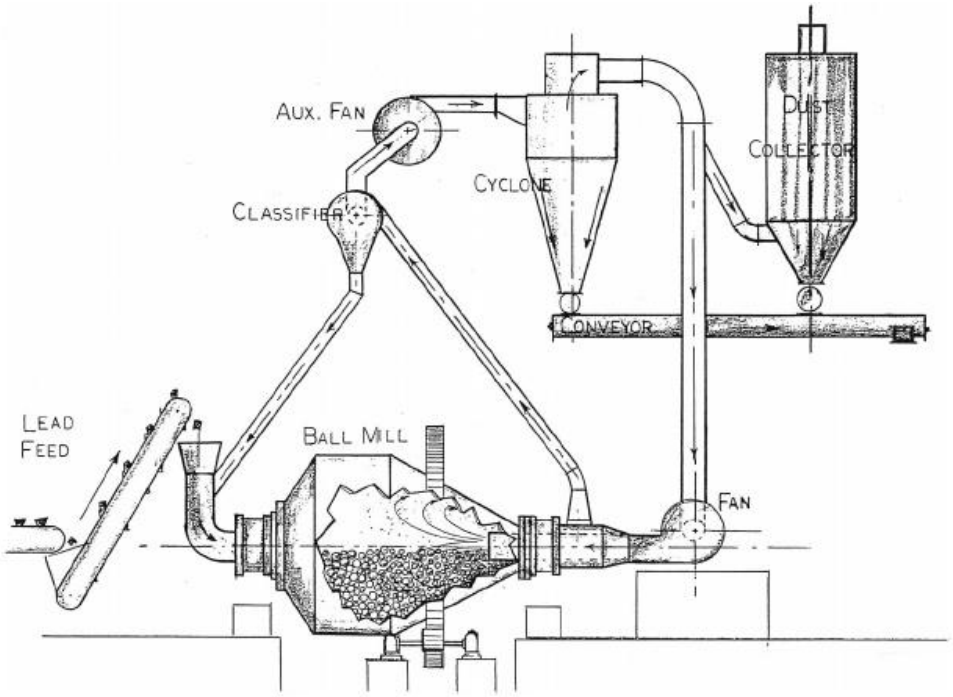

Figure 2.3: Typical Ball Mill system [18].

Characteristics of PbO being produced by Ball Mill and Barton processes are displayed in Table 2.3.

Table 2.3: Characteristics of PbO produced by Barton and Ball Mill processes [18].

Characteristics	**Barton Pot**	**Ball Mill**
Particle Size	3 to 4 µm mean diameter	2 to 3 µm mean diameter
Oxide crystal structures (wt%)	5 to 30% β-PbO (typ.) remaining α-PbO	Essentially 100% α-PbO
Surface Area (m^2/g)	0.7	2.0 to 3.0
Free lead content (wt%)	Approx. 18 to 28	Approx. 25 to 35

2.2.5 Synthetic approaches for nanoparticles of PbO

Recently, the synthesis of nanostructural oxide materials has attracted considerable attention of researchers globally. Lead oxide based compounds consist of many crystalline forms such as PbO (α, β), Pb_2O_3, Pb_3O_4, and PbO_2 (α, β). As discussed before, PbO_2, which is used as a positive active material in lead acid battery, has been extensively studied, meanwhile, PbO is the starting precursor for both positive and negative electrode materials, which is then converted to active PbO_2 and Pb respectively during cell formation process in both electrodes. The interest to improve the characteristics of PbO to obtain more discharge capacity and long cycle-life is immense as it is expected that PbO in the form of nano-particulates is able to deliver more electrical energy during discharge process due to its large specific surface area and good reversible property [15].

Over the years, nanostructured PbO has been synthesized and investigated via spray pyrolysis, hydrothermal method, sonochemical, and electrochemical deposition and chemical solution method to enhance the discharge capacity, charge acceptance and operating life of lead-acid battery.

2.2.5.1 Spray pyrolysis technique

Spray pyrolysis technique (SPT) has been one of the methods adopted to synthesize nanostructured PbO for research in lead-acid battery. Since the last three decades, SPT

has also been one of the major techniques to deposit a wide variety of materials in thin film form. The prime requisite for obtaining thin film with good quality is the optimisation of preparation conditions like substrate temperature, spray rate, concentration of solution etc. However, in recent years an emphasis has been given to a variety of atomization techniques such as ultrasonic nebulisation, improved spray hydrolysis, corona spray pyrolysis, electrostatic spray pyrolysis and microprocessor based spray pyrolysis. All these are most critical in controlling over the size of the droplets and their distribution over the preheated substrates [9, 20].

Meanwhile, PbO thin films were prepared via the spray pyrolysis of aqueous lead salt solution and deposited onto a heated lead substrate. A homogeneous coating obtained at 260 ^{o}C consisted of well-crystallized α-PbO as starting precursor of lead-acid electrode material. After formation, dense agglomerates of β-PbO_2 particles were accompanied by unreacted α-PbO. Preliminary electrochemical tests of the cell revealed a progressive decrease in polarization during charging in the first few cycles probably associated to improved adherence of active particles to the substrate. The cell was found to maintain a discharge capacity of ca. 100 mAh/g (40% of the theoretical value) upon extensive cycling. Nevertheless, the technique is only limited to thin film application and small production capacity with expensive organic solvent applied as well as sintering heat is needed in the synthesis process which directly increases the cost of production.

2.2.5.2 Sonochemical method

There are many reports about the effect of ultrasonic waves on morphology and particle size of PbO in synthesized solutions. In a great number of reports, ultrasonic affected synthesized solution is called “sonochemical solution” and the synthesis method used is called ‘‘sonochemical method’’ [21]. The ultrasonic waves effect on the synthesis system in different ways. The ultrasonic effect strongly depends on system species and reaction mechanism. It has been reported that this method is an effective way of stabilizing the nanometer-sized particle produced during the synthesis [22]. The first and simplest effect of ultrasonic waves on synthesized solutions is a stop on particle growth and breakage of agglomerated and colonial balks of small particles.

Lead salt solution reacts with alkaline solution to produce PbO in the presence of ultrasonic waves to prevent the agglomeration and growth of PbO nanoparticles formed with the help of surfactants as structure director additive for acquiring unique morphology and uniform particle size. Hence, the prepared PbO via this method can deliver 140 mAh/g of electrical energy as positive active material during discharge of the electrode. Yet, this process will consume significant amount of costly surfactants for large scale production while the capacity performance acquired by the prepared PbO is almost comparable with the existing process, where conventional PbO is able to deliver up to135 mAh/g.

2.2.5.3 Hydrothermal method

In addition to the previous methods, nanostructured PbO has been synthesized via hydrothermal method in which chemical solution method is initially carried out to produce desired lead salt and followed by the decomposition of the salt at high temperature to obtain nanostructured PbO. The said lead salts reported for the decomposition process are lead nitrate ($Pb(NO_3)_2$), lead hydroxide ($Pb(OH)_2$), lead carbonate ($PbCO_3$), lead bromide ($PbBr_2$), lead citrate, lead oxalate and lead coordination polymer [11]. The long list of these lead salt products has indicated that tremendous investigations have been conducted in this area to produce nanostructured PbO with outstanding performance.

Moreover, one of the attractive reasons that this method is popularly adopted is due to the process compatibility in recycling PbO from scrap battery paste which would significantly reduce the cost of raw material. This process is energy efficient when compared to the conventional method of producing PbO. When it is applied in PbO recovery from scrap battery, there are numerous reports on the purity of the material is acquired. There are literally few reports showing the electrochemical efficiency of the synthesized product in lead-acid cell [12]. The process is only successfully established at a small scale like pilot plant for operation due to expensive lead salt solutions, inefficiency in handling chemical by-products in its early stage, and the decomposition at sintering temperature of 400 ^{o}C, All these might end up producing PbO with comparable cost to that of commercial PbO. Nevertheless, this synthesis method could

be the game changer to the existing technology when either the cost or electrochemical performance of the synthesized material is significantly improved.

2.2.5.4 Electrodeposition

Nanostructured PbO is rarely synthesized via electrodeposition method. Till date, only one study reported in investigating the nanodenderitic morphology of PbO formed via the electrodeposition of lead salt solution onto planar glassy carbon electrode with the assistance of polyethylene glycole as soft template [6]. This study revealed significant information on how nanodendritic morphology of PbO formed with preferential direction, but not its performance in lead-acid cell. This method enables to explore numerous novel morphologies of nanostructrured PbO_2 with high active surface area, especially those with dendritic shapes which have shown prevailing performance when tested in lead-acid cell [13]. Nonetheless, scalability of this method is limited by current engineering technology.

2.2.5.5 Chemical solution method

Nanostructured PbO synthesized via chemical solution method was first reported in 1922 [10] by reacting lead salt solution with various concentration of sodium hydroxide as well as potassium hydroxide to precipitate different forms of PbO. However, the subsequent studies were only conducted to study its purity, density, solubility in acidic or alkaline solution, crystallographic measurement and exploring the evidence of other

possible forms of PbO which is black under visual inspection [11]. On the other hand, the relationship of nanostructured PbO synthesized via this method with respect to its electrochemical performance in lead-acid cell is greatly neglected over the years.

As this method is simplistic in design to produce nanostructured PbO with potential microstructural parameters, and the method is readily compatible to the existing process of lead-acid battery technology, also implementable in the last process of PbO recovery from scrap battery paste. Thus said, an alternative synthesis method based on a feasible chemical solution synthesis to produce nanostructured PbO needs to be comprehensively explored. Furthermore, the synthesized PbO will be used as starting precursor to form unique active material of lead-acid cell via the existing manufacturing process of electrochemical oxidation in the presence of inorganic or organic electrolyte.

In this study, lead nitrate and sodium hydroxide solutions were used in the synthesis of nanostructured PbO. Lead nitrate solution was selected due to its high solubility in solution which could achieve 30% of its overall solubility. Meanwhile, sodium hydroxide was chosen because of its high reactivity for the formation of the final product within a short duration.

2.3 Lead Dioxide (PbO_2)

2.3.1 General application

Lead dioxide occurs in nature as the mineral plattnerite. It is used as an oxidizing agent in manufacturing dyes and intermediates. It is also used as a source of oxygen in matches, pyrotechnics, and explosives. In matches, the oxide is combined with amorphous phosphorus as an ignition surface. It is also used in making lead pigments, liquid polysulfide polymers and rubber substitutes. Lead dioxide electrodes are used in lead-acid storage batteries in which lead dioxide accumulates on positive plates.

2.3.2 Physical properties

Lead dioxide is exhibiting red tetragonal crystals or brown powder; density 9.64 g/cm^3; decomposes on heating at 290°C; practically insoluble in water; also insoluble in alkalis; moderately soluble in hydrochloric acid and also, in nitric acid-hydrogen peroxide mixture; slowly dissolves in acetic acid.

2.3.3 Thermochemical properties

The thermochemical properties of PbO_2 are indicated in Table 2.4 below.

Table 2.4: Thermochemical properties of PbO_2 [19].

Thermochemical Properties	**Energy**
ΔH_f^o	-66.30 kcal/mol
ΔG_f^o	-51.94 kcal/mol
S^o	16.40 Cal/degree mol
C_p	15.44 Cal/degree mol

The enthalpy energy of formation of PbO_2 stands at -66.30 kcal/mol, while standard free energy of formation is -51.94 kcal/mol. The standard entropy and heat capacity of PbO_2 are 16.40 Cal/^{o}C mol and 15.44 Cal/^{o}C mol respectively.

2.3.4 General preparation of PbO_2

Lead dioxide is produced by oxidizing an alkaline slurry of lead monoxide with chlorine, sodium hypochlorite, or bleaching powder. Alternatively, it is obtained by passing chlorine into a hot aqueous suspension of lead sulfate and magnesium hydroxide.

Moreover, it is also produced by electrolysis of acidic solutions of lead salts using a lead or platinum electrode. In such electrolytic process, lead dioxide is deposited on the anode of the cell. Insoluble powdered lead dioxide also may be obtained, when lead tetroxide is heated with nitric acid. Lead dioxide also can be prepared by fusing lead monoxide with a mixture of sodium nitrate and sodium chlorate [19].

In lead-acid battery, lead monoxide is used as the precursor to form lead dioxide in the positive plate by electrochemical oxidation in sulfuric acid solution.

2.3.5 Electrochemical properties of PbO_2

The physical and electrical properties of PbO_2 is stated as below:

Table 2.5: Physical and electrical properties of PbO_2 [2].

Parameters	Alpha - PbO_2	Beta - PbO_2
Density (g cm^{-3})	9.1-9.4	9.1-9.4
Pore Size (nm)	<60	<10
Crystallite Size (nm)	55	20
BET Surface area (m^2 g^{-1})	0.48	9.53
Discharge Capacity (Ahg^{-1})	0.135	0.164

In accordance to the processes that occur during the formation stages and taking into account that α-PbO_2 is formed in weak acidic to alkaline media, whereas β-PbO_2 is formed in acidic media, the following overall equation for the β-PbO2: α-PbO2 ratio in the active mass at the end of the formation process has been proposed:

$$\beta\text{-}PbO_2 : \alpha\text{-}PbO_2 = (q^0_{PbSO4} + q^1_{PbSO4} + q^1_{PbO}) : (q^0_{PbO} + q^1_{PbSO4} + q^1_{PbO}) \quad \text{-Equation 2.6}$$

where q^0_{PbSO4} is the initial quantity of $PbSO_4$ in the basic lead sulfates; q^1_{PbSO4} is the amount of $PbSO_4$ produced during soaking and the first formation stage; q^1PbO is the amount of PbO transformed into β-PbO_2, a process which may proceed at the end of the first formation stage; q^0PbO is the total initial amount of PbO (free and bonded in basic lead sulfates).

Numerous scientists have investigated the influence of the β-PbO2: α-PbO2 ratio on the capacity of plates and established that this ratio does indeed affect capacity, but there is no direct correlation. In one experiment, two series of plates were produced using pastes with the same acid-to-oxide ratio in the range of 0–12%, but mixed at two different temperatures, namely, 30^{o}C to yield tribasic lead sulfate (3BS) crystals and 80^{o}C to facilitate the formation of tetrabasic lead sulfate (4BS) crystals. Note that, 3BS and 4BS pastes form different positive active material (PAM) structures. If the capacity was determined directly by the β-PbO_2: α-PbO_2 ratio, then both series of plates should have the same capacity determined only by this ratio. The result shows that the β-PbO_2: α-PbO_2 ratio is the same for the two series of plates, when the acid-to-oxide ratio in the paste is up to 8%.

On the other hand, the higher the discharge current, the weaker is the dependence of the plate capacity on the β-PbO_2: α-PbO_2 ratio. Although the β-PbO_2: α-PbO_2 ratio for a given acid-to-oxide ratio is the same, the active mass prepared from pastes containing 3BS yields a higher capacity than plates produced with 4BS pastes. Thus, the capacity of the active mass depends not only on the ratio between the two PbO_2 modifications in PAM, but also, and much more so, on the type and structure of the PAM that are determined by the type of basic lead sulfates in the paste subjected to formation. Hence, the capacity of the positive plate is determined by the structure of the active mass and the relative proportions of β-PbO_2 and α-PbO_2 [2].

Chapter 3

3.0 Materials

A list of chemicals, reagents and substrates are described as follows:

a) Lead nitrate powder, $Pb(NO_3)_2$ (Systerm Chemicals)

b) Sodium hydroxide pallets, NaOH (Systerm Chemicals)

c) Sulfuric acid, H_2SO_4 [4.7 M] (R & M Chemicals)

d) Negative active material, basic lead sulfate (Yokohama Batteries)

e) Lead alloy substrate (98% Purity) (Yokohama Batteries)

f) Commercial pure PbO (Yokohama Batteries)

g) Distilled water (18.2 Mohm) was used throughout the study.

3.1 Methodology

A facile synthesis of flower-like PbO via one-pot chemical synthesis of lead (II) nitrate solution ($Pb(NO_3)_2$) with sodium hydroxide solution (NaOH) in the absence of any structure director additive under vigorous stirring condition at room temperature was systematically conducted. The as-synthesized PbO was dried and used as starting

material to form active paste by mixing with DI water and dilute sulfuric acid. The pasted and dried active paste was then electrochemically oxidized in 4.7 M sulfuric acid (H_2SO_4) to form nanodendritic PbO_2. The steps were repeated for commercial pure PbO to produce bulk PbO_2 as the control sample.

In this experiment, the as-synthesized PbO and electrochemically oxidized PbO_2 as well as commercial pure PbO and bulk PbO_2 were characterized by X-ray powder diffraction (XRD) and scanning electron microscopy (SEM). The electrochemical properties of PbO_2 were investigated by cyclic voltammetry (CV) and constant current charge/discharge methods. Moreover, the acquired electrochemical results were compared with those of PbO_2 formed by using commercial pure PbO as starting material and found that the electrochemically oxidized nanodendritic PbO_2 was predominant in electrochemical property and would become one of the promising electrode materials for next generation of lead-acid battery or other LAESD.

3.2 Synthesis of nanostructured PbO

$Pb(NO_3)_2$ solution was prepared and reacted with NaOH solution at a molar ratio [$Pb(NO_3)_2$: NaOH] of 0.4 under vigorous stirring by magnetic bar for 15 min. The yellow greenish precipitate was filtered and washed with excess distilled water and acetone before drying in an oven at 50 ^oC for 24 hours. The dried powder was kept in a sealed container for material characterization. Besides, bulk volume of this nanostructured PbO

was synthesized and used as a precursor in fabricating a few random commercial 12V automotive batteries for product characterization.

3.3 Synthesis of nanostructured PbO_2

The as-synthesized PbO was then mixed with DI water and 4.7 M H_2SO_4 at a weight ratio of [PbO: DI water: H_2SO_4 = 10 : 3 : 1]. The mixture was stirred for 15 min to produce active mixture for pasting. The active mixture was then pasted onto a lead alloy cavity of 0.5 cm^2 followed by drying in an oven at 50 ^oC for 24 h. The dried electrode was used as positive electrode and assembled into a battery cell with a negative electrode consisted of cured active material (supplied by Yokohama Batteries, Malaysia) while separated by an absorbed glass matt with zero gap distance. The assembled battery cell was soaked in 4.7 M H_2SO_4 for 2 h and then charged at constant voltage of 2.48 V for 48 h [12] to form PbO_2 in positive electrode. The positive electrode was later dismantled from the cell and cleaned with excess acetone. The electrochemically oxidized PbO_2 in the cavity (0.5 cm^2) was dried and kept in an air tight container for material characterization. The steps were repeated for commercial pure PbO to produce bulk PbO_2 as the control sample.

3.4 Characterization methods

3.4.1 X-ray diffractometer (XRD)

X-ray diffraction methods are the most widely-used methods for determining the crystal structure of materials which identify respective chemical compounds and product quality rather than their compositions of chemical elements.

X-ray diffractometry is a spectroscopic type of diffraction method that depends on phenomenon of wave interferences. According to Bragg's Law, electromagnetic waves of X-ray beams incident on a crystallite solid will be diffracted by the crystallographic planes as illustrated in Figure 3.1. Two in-phase incident waves, beam 1 and beam 2, are deflected by two crystal planes (A and B). The deflected waves will not be in-phase except when the following relationship is satisfied [30].

$$n\lambda = 2d \sin \theta \qquad \text{- Equation 3.1}$$

where:

n = order of reflection

λ = wavelength of the x-rays

d = characteristic interplanar spacing

θ = angle between the incident beam and the normal to the reflecting lattice plane

Equation (3.1) is the basic law of diffraction called Bragg's Law and it can be simply acquired by calculating the path differences between the two beams in Figure 3.1. The path difference depends on the incident angle (θ) and the spacing between the parallel crystal planes (d). In order to keep these beams in-phase, their path difference (SQ + QT = 2d sin θ) has to equal one or multiple X-ray wavelengths (nλ) [30].

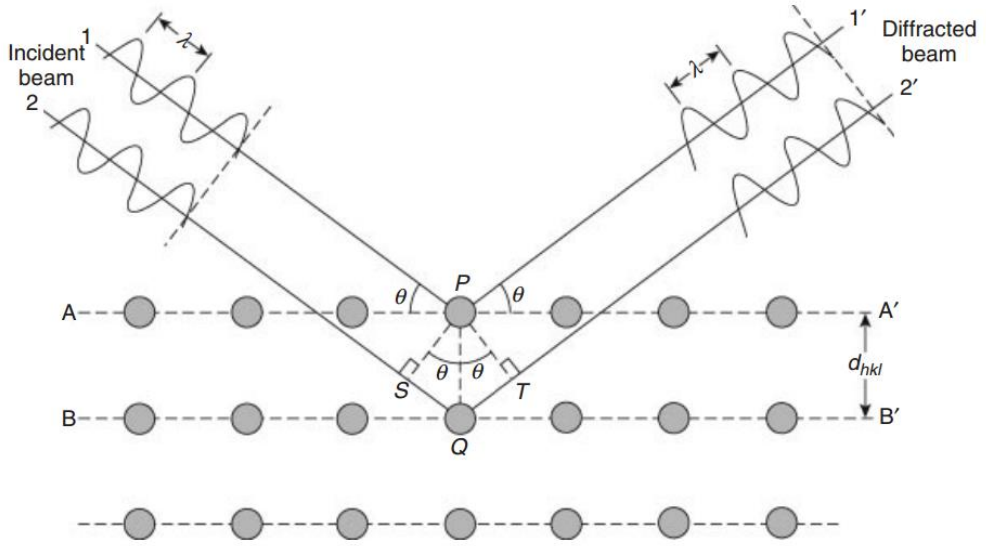

Figure 3.1: Bragg diffraction by crystal planes [31].

According to Bragg's Law, when constructive interference is detected at a given incident angle and a wavelength of the incident beam, information on the spacing between atomic planes of a crystal can be obtained. Knowing the spacings of crystallographic planes by diffraction methods, crystal structure of materials can be determined [30].

The XRD of dried powder from sections (3.2) and (3.3) and commercial pure PbO were characterized by using an X-ray diffractometer X'PERT PRO PW3040 (Cu Kα radiation and wavelength, λ = 0.154 nm) for product quality. Typical geometric arrangement of X-ray diffractometer is illustrated in Figure 3.2.

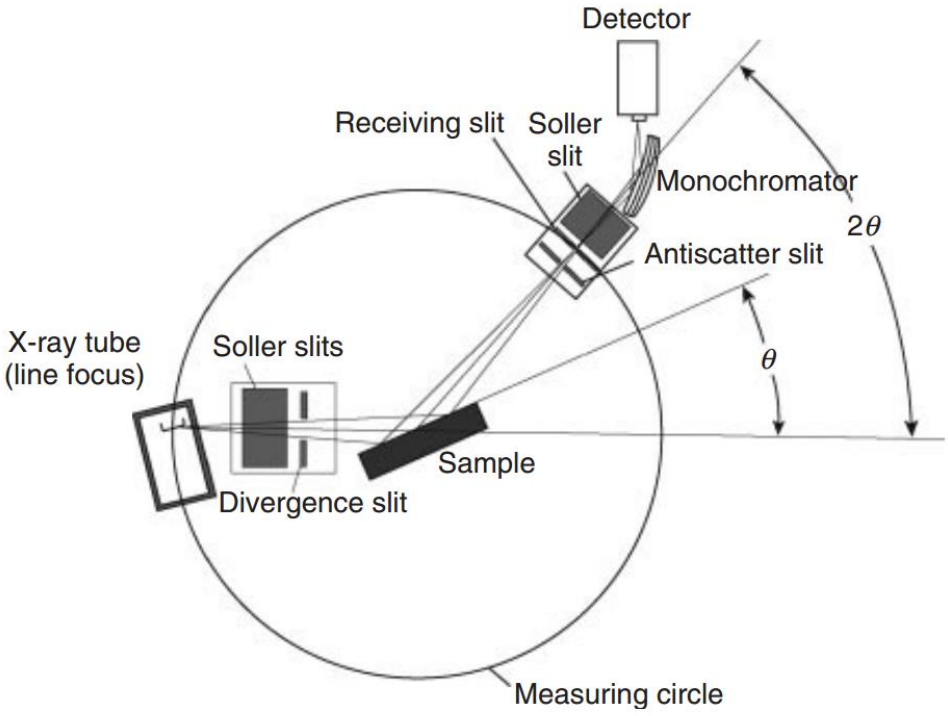

Figure 3.2: Geometric arrangement of X-ray diffractometer [31].

3.4.2 Scanning electron microscopy (SEM)

The scanning electron microscope (SEM) is the most widely used type of electron microscope. It examines microscopic structure by scanning the surface of materials, similar to scanning confocal microscopes but with much higher resolution and much greater depth of field. In comparison to the wavelength of light (5×10^{-7} m), electrons have much shorter wavelengths of between 1×10^{-11} m to 1×10^{-12} m with respect to the accelerating voltage applied, which allows for better resolution up to 1 nm in an electron microscope than that of conventional optical microscopes.

In such measurements the surface is invariably solid, so raster pattern for scanning is possible. Several signals such as backscattering (BSE), secondary (SE) and Auger electrons, X-ray fluorescence photons are originated. The first two signals like back scattering and secondary emissions are most useful for analysis. They serve as basis for SEM [31].

A schematic representation of SEM is displayed in Figure 3.3 involving the use of common electron gun source. The focusing system comprises condenser (1) and objective lens (2) to facilitate reduction of an image (~200 nm). Condenser lenses (1) which permit electron beam to reach objective lens (2) and ultimately reaching to sample (3). Now SEM is achieved by two coils. These coils deflects beam in $x < y$ direction. Scanning is controlled by electronic signal on one coil (4) in the line scan. Left coil (5) is used to deflect beam. This helps to irradiate sample with electrons beam. The signal (digital or analog) from specimen is stored in the digital form (6). Same signal

permits movement of cathode ray tube as displayed (6). The (7) magnification is obtained by the width of display divided by the width of signal [32].

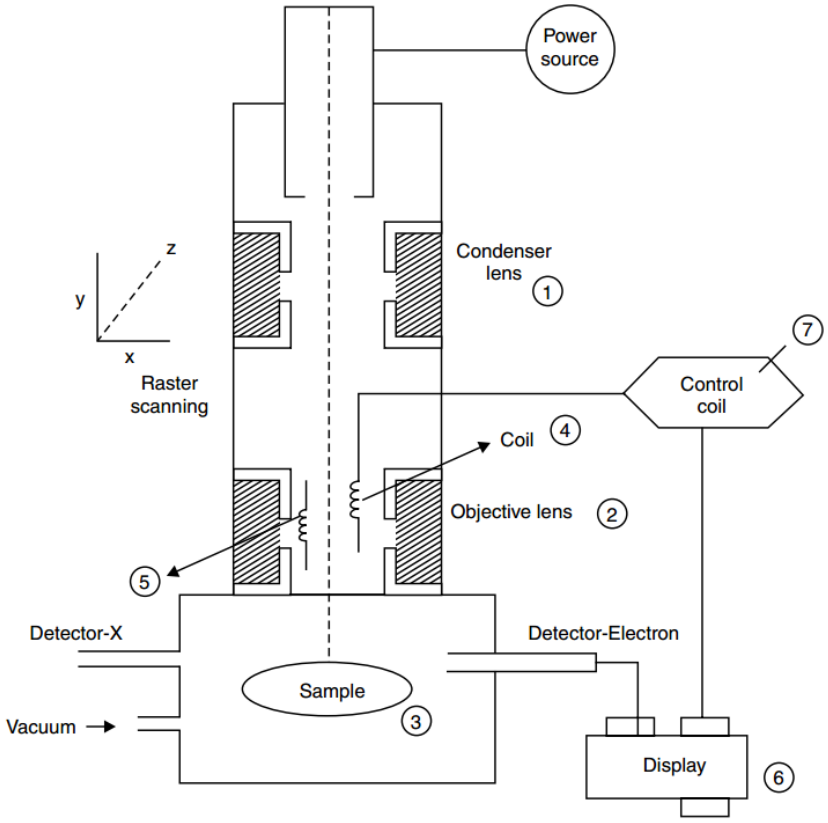

Figure 3.3: Schematic representation of SEM [32].

Additionally, a commonly used detector in an SEM is the Everhart-Thornley (E-T) detector, as illustrated in Figure 3.4. The SEs travel with large deflection angles toward the detector, while BSEs travel directly toward the detector. The Faraday cage in the front of the detector is either positively or negatively charged (250 or −50 V), depending on signal selection. When given a positive charge, the detector attracts signal electrons,

particularly, SEs. When given a negative charge, it can screen out SEs with energy less than 50 eV. The key element of the E-T detector is the scintillator, a disk of about 8 - 20 mm in diameter. The scintillator converts signal electrons into photons by accelerating the electrons with +12 kV and striking them onto a disk. The photons then travel through a light guide and enter the photomultiplier tube for signal gain (up to ~106×). The photomultiplier output is further amplified for display on a display screen [31].

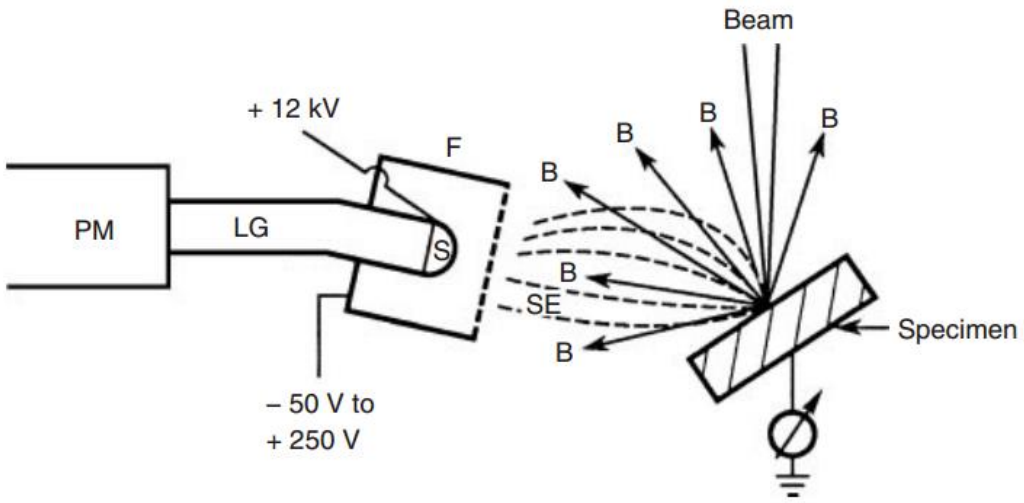

Figure 3.4: Signal collection by the Everhart-Thornley detector. B, backscattered electron trajectory; SE, secondary electron trajectory; F, Faraday cage; S, scintillator; LG, light guide; PM, photomultiplier tube [31].

In this project, the SEM images of dried powder from section (3.2) and (3.3) and commercial pure PbO were also characterized by SEM (FEI Quanta-400 FESEM) for microstructural analysis.

3.4.3 Potentiostat

Potentiostat is the most important component of any voltammetric devices in monitoring current at fixed voltage. This equipment is fundamental to modern electrochemical studies using three electrode systems for investigations of reaction mechanisms related to redox chemistry and other chemical phenomena. It contains an integrated circuit operation operational amplifier and digital modules. A typical electronic circuit for potentiostat is illustrated in Figure 3.5. The output of Amplifier (1) is contacted to counter electrode with feedback to its own inverting output through the reference electrode. The feedback decreases with the difference between the inverting input and noninverting input amplifier and leads to the establishment of same potential as Entrance of amplifier I. Since difference in two electrodes is zero, the reference electrode is connected to Entrance through high impedance. In amplifier 3, the current flows in counter electrode. The three-electrode set up is preferred (from micro to milliamp scale). With microelectrodes, the current is in the range of 10^{-9} to 10^{-12} ampere. The operational amplifier acts as a current to voltage converter (amplifier 2) to supply output signal to converter [32].

Most voltammetric methods are dynamic. Exact control of the potential is a critical function of potentiostat. With digital electrons, most of them work in digital pattern. Digital fabrication of the applied voltage has given rise to pulsed voltammetry. The latter is fast and sensitive. A commonly used wave form model is used. Potentiostat is essential, if one prefers to use micro and nanometer size electrodes involving pico or nano ampere range current. Square wave polarography needs rapid response period from the electronics. Wide range of potentiostats is available in the market [32].

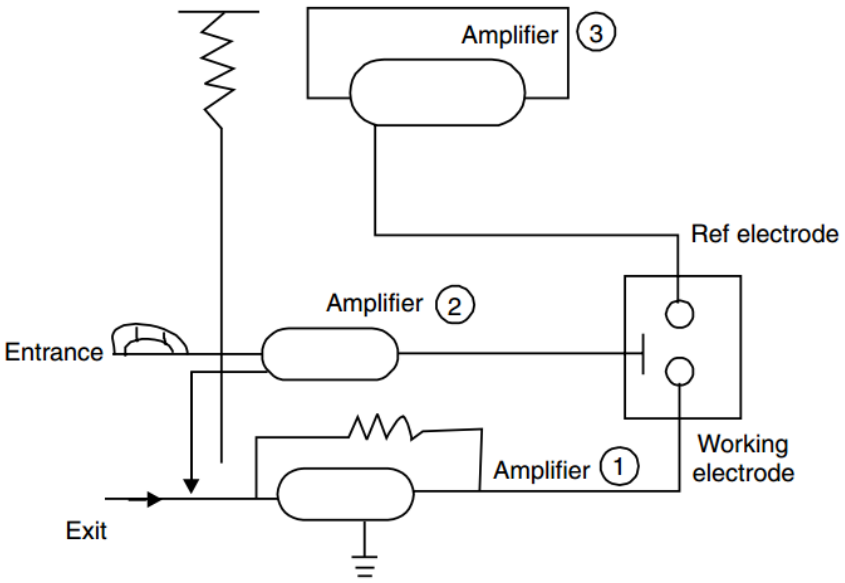

Figure 3.5: Typical electronic circuit for potentiostat [32].

Electrochemical tests of this project were conducted by using Autolab PGSTAT302N in a classical three-electrode cell containing 4.7 M H_2SO_4 where the electrochemically oxidized PbO_2 was used as the working electrode, while platinum mesh (25 X 35mm, 80 mesh) as the counter electrode and Hg/Hg_2SO_4/saturated K_2SO_4 as the reference electrode. Cyclic voltammetry (CV) measurements were conducted at a scanning rate of 10 mV/s from 0.6 - 1.6 V. Meanwhile, the initial discharge behavior was investigated by discharging the working electrode at a current density of 200 mAg^{-1} until its potential decreased to 0.65 V. All experiments were carried out at room temperature unless stated otherwise.

3.4.4 Characterization of Battery Product

There are numerous industrial standards to be complied by battery manufacturers to ensure the final battery product is ready for delivery to customers. These standards include Japanese Industrial Standard (JIS), British Standard (BS EN), Deutsches Institut für Normung Standard (DIN), International Electrotechnical Commission Standard (IEC) and so forth. As JIS D 5301 [33] is a widely known industrial standard in automotive battery industry, it was used as the product characterization in this study.

In battery product characterization, there are two most essential rating tests for evaluating the long-term electrochemical performance and durability of the battery product. These two rating tests are:

1) Capacity rating: Ampere hour (Ah) rating over 20 hours (C20).
2) Cold cranking ampere (CCA) rating: To evaluate CCA capability via high rate discharge.

Thus, Ah rating indicates the ability of a battery to deliver current for an extended period of time. Ambient temperature is one of the factors to influence the ampere-hour rating of a battery. Usually, a battery at low temperature has a lower ampere hour rating than that in warm climate.

The capacity of automotive batteries is rated at 20 hours which means that the battery should last for the stated duration when discharges at a given current. For instance, a battery with capacity of 35 Ah should last for 20 h as it discharges at a current of 1.75A.

Till that point, the cut-off voltage of each cell will be 1.75V (or 10.5V for a 12V battery, or 5.25V for a 6V battery). Normally, the larger the battery plates that filled with more active material, the greater the ampere-hour rating is over a given duration.

According to JIS, three cycles of the C20 were conducted to evaluate the capacity of a battery. The first two cycles of C20, each cycle would require any fresh commissioned battery to fulfill at least 90% of its nominal capacity while the third cycle would need at least 100%.

CCA rating shows how good a battery is able to provide high cranking current in a low temperature environment and to predict the nominal cycling ability of a battery. This rating is dependent on the number and surface area of the battery plates or active material used. For example, a battery temperature of -18 ^{o}C is discharged at a given high rate current while voltage reading is measured during the discharge.

According to JIS, CCA rating is conducted in two consecutive steps where a battery, conditioned at temperature of -18 ^{o}C, is discharged at initial high stated current with respect to battery model for 30 second, and followed by second discharge current (60% of the first discharge current) till the cut-off voltage of the battery reaches 6V. During the first current discharge, final voltage after 30 second was compared while the duration of the second current discharge till stated cut-off voltage was monitored for distinction between battery performance.

If a battery passes CCA rating, it indicates that the electrochemical performance of the battery is able to provide high current under a bad climate condition and to operate well beyond the nominal life cycle under normal operating condition.

In this study, the fabricated batteries with designated amount of as-synthesized nanostructured PbO, were subject to C20 (three cycles) and CCA (at -18 ^{o}C) rating tests. The rating tests were carried out at Yokohama Batteries Sdn Bhd. As the amount of as-synthesized PbO was very limited, only five battery samples were prepared at arbitrary amount for the tests. Table 3.1 shows the characteristics of battery samples being prepared with different amount of as-synthesized nano PbO in positive and negative plates respectively.

Table 3.1: Characteristics of Prepared Battery Samples.

No.	**Category**	**Sample 1 (Raw Battery Sample)**	**Sample 2**	**Sample 3**	**Sample 4**	**Sample 5**
1	Label	NS60	40B24-N20	40B24-N100	40B24-P50	40B24-P100
2	Battery Model (Nominal Capacity)	40B24-9plates (35 Ah)	40B24-9plates (35 Ah)	40B24-9plates (35 Ah)	40B24-9plates (35 Ah)	40B24-9plates (35 Ah)
3	Positive Plate Characteristics	Conventional Plate (Ball Mill Oxide)	Conventional Plate (Ball Mill Oxide)	Conventional Plate (Ball Mill Oxide)	50% Nano PbO + 50% Ball Mill Oxide	100% Nano PbO
4	Negative Plate Characteristics	Conventional Plate (Ball Mill Oxide)	20% Nano PbO + 80% Ball Mill Oxide	100% Nano PbO	Conventional Plate (Ball Mill Oxide)	Conventional Plate (Ball Mill Oxide)

Chapter 4

4.0 Results and discussion

4.1 Material phase and purity

Figure 4.1a and 4.1b show the XRD patterns of as-synthesized PbO prepared in the absence of structure director additive and commercial pure PbO respectively. Both diffraction peaks can be perfectly indexed with a mixture of orthorhombic and tetragonal structures. β-PbO (orthorhombic) is mostly observed in Figure 4.1a while majority of α-PbO (tetragonal) can be seen in Figure 4.1b. As opposed to conventional chemical synthesis of producing pure nanostructured lead oxide [12, 23], the presence of structure director additive and heating process to decompose lead hydroxide ($Pb(OH)_2$) to PbO are not needed as the synthesis process is conducted at lower molar ratio of $Pb(NO_3)_2$ to NaOH so that the synthesis medium is always maintained at pH 14 as the formation of $Pb(OH)_2$ at this alkalinity is unstable and readily transformed to PbO [24] which can be observed clearly in Figure 4.1a.

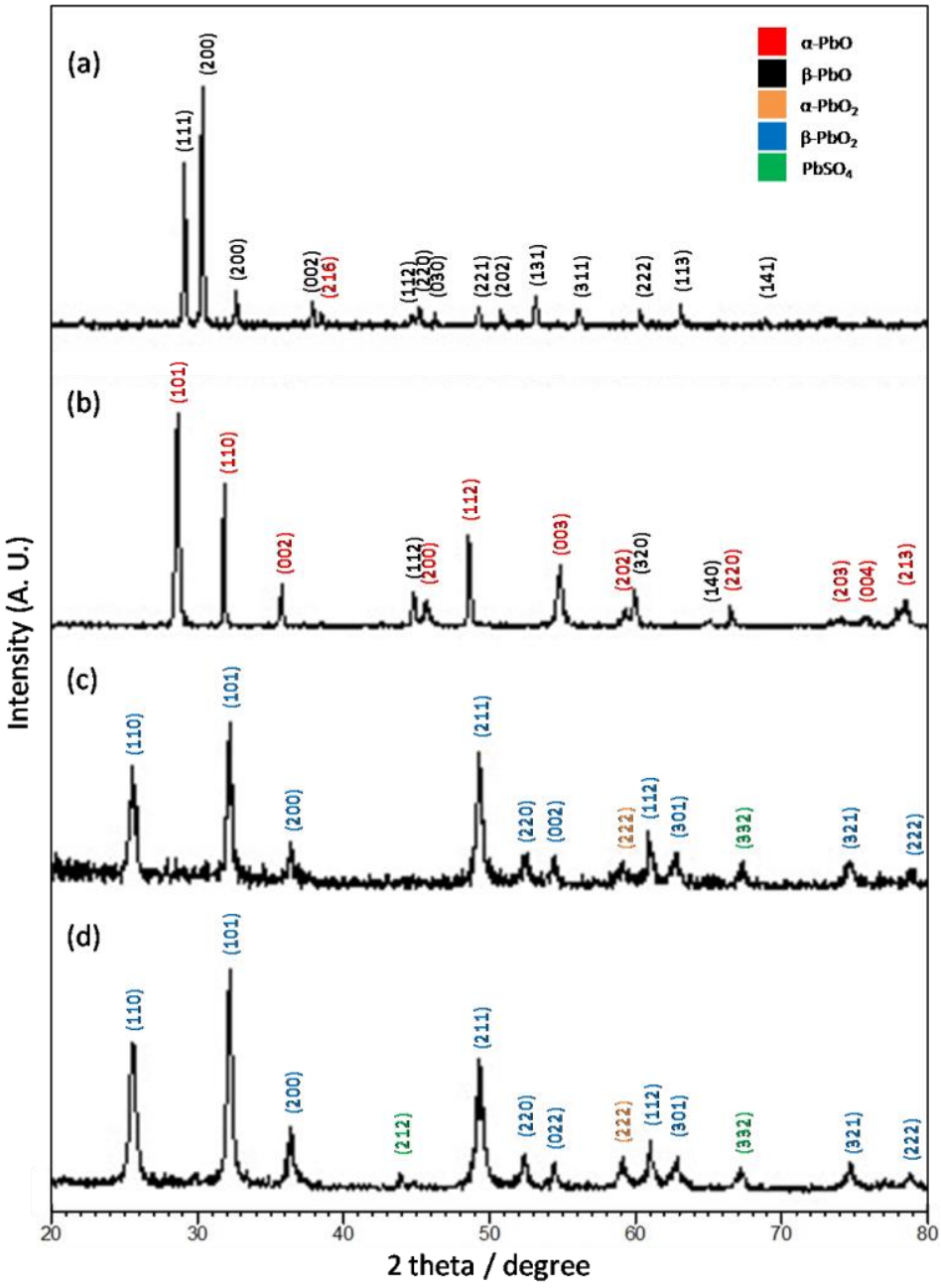

Figure 4.1: (a) XRD patterns of as-synthesized PbO prepared in the absence of structure director additive and (b) commercial pure PbO, (c) PbO_2 produced via electrochemical oxidation of active mixture composed of as-synthesized PbO and (d) bulk PbO_2 synthesized by using commercial pure PbO.

Meanwhile, Figure 4.1c and 4.1d show the diffraction peaks of nanodendritic PbO_2 produced via electrochemical oxidation of active mixture composed as-synthesized PbO, and bulk PbO_2 formed from active mixture consisted of commercial pure PbO, respectively. Both samples contain majority of β-PbO_2 while small amount of α-PbO_2 and lead sulfate are observed. All four distinctive diffraction peaks in Figure 4 indicates that the samples are highly crystalline.

4.2 Morphology

Figure 4.2a and 4.2b indicate SEM images of as-synthesized flower-like PbO and commercial pure PbO. As can be seen in Figure 4.2a, the flower-like PbO is formed with three dimensional networks of nanoflakes. The thickness of each nanoflake ranging from 250-280 nm is seen in higher magnification of SEM image (inset of Figure 4.2a), while its length is from 2 - 36 µm. The formation of nanoflake PbO leading to the growth of flower-like structure is anisotropic. The growth mechanism of nucleic proceeds spontaneously with high activation energy based on periodic bond chain (PBC) theory [25] where flat crystal growth is dependent on a discontinuous surface [26]. Besides that, Figure 4.2b shows lumps of PbO particles ranging from 5 – 10 µm which is composed fine particles on the surface (less than 250 nm as can be seen in the inset of Figure 4.2b).

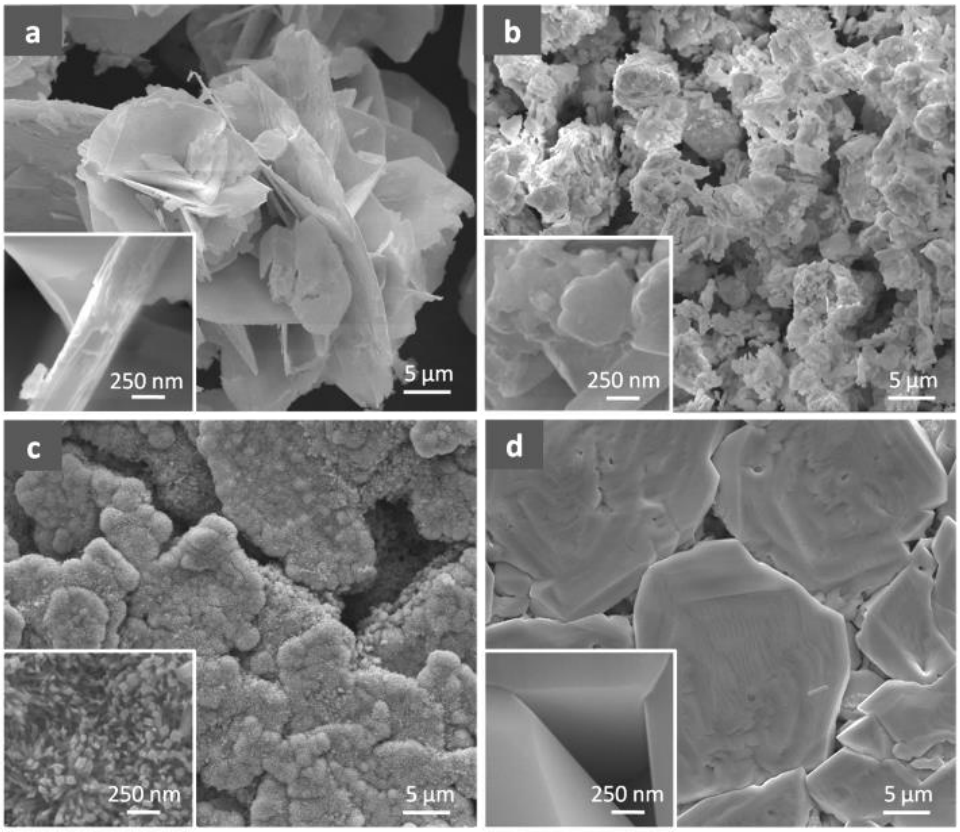

Figure 4.2: SEM images of (a) as-synthesized nanostructured PbO and (b) commercial pure PbO, (c) nanodendritic PbO_2 formed from active mixture composed of (a), (d) bulk PbO_2 formed from active mixture composed of (b).

Moreover, Figure 4.2c is showing SEM image of nanodendritic PbO_2 formed via electrochemical oxidation of active mixture composed of as-synthesized PbO, while Figure 4.2d is the image of bulk PbO_2 formed from active mixture of commercial pure PbO. The inset of Figure 4.2c demonstrates that uniform nanodendrites are formed on the agglomerated PbO_2 with each diameter less than 50 nm. The formation of nanodendritic PbO_2 in Figure 4.2c on the primary surface of agglomerated PbO_2 suggesting that flower-like PbO, which is formed from crystal growth of discontinuous

surface, when it is subject to electrochemical oxidation at constant voltage in the presence of electrolyte, the growth mechanism would follow an adapted diffusion limited growth pattern model [27] where random particles would grow on a seed particles preferentially and anisotropically leading to the formation of uniform nanodendritic PbO_2. Meanwhile, only bulk PbO_2 particles are formed without dendritic rods after the formation process as can be observed in Figure 4.2d when conventional pure PbO is used as starting precursor.

4.3 Electrochemical property of prepared samples

Figure 4.3a reveals cyclic voltammograms of bulk PbO_2 particles and nanodendritic PbO_2 in 4.7 M H_2SO_4 at 20^{th} cycle and scanning rate of 10 mV/s in the potential range between 0.6 and 1.6 V. The obtained CV curves are similar to those acquired elsewhere [28]. The oxidation of $PbSO_4$ to PbO_2 can be observed at the anodic peak of 1.4 V (VS. Hg/Hg_2SO_4 in sat. K_2SO_4), while the oxidation of oxygen occurs beyond 1.5 V, followed by the reduction of PbO_2 to $PbSO_4$ at the cathodic peak of 0.93 V. The curves show that the cathodic current is much higher than the anodic current. By comparison, the CV curve of nanodendritic PbO_2 shows higher current density than that of bulk PbO_2 particles and this might be attributed to high surface area and better network contact of nanodendritic particles for fast charge transfer [29].

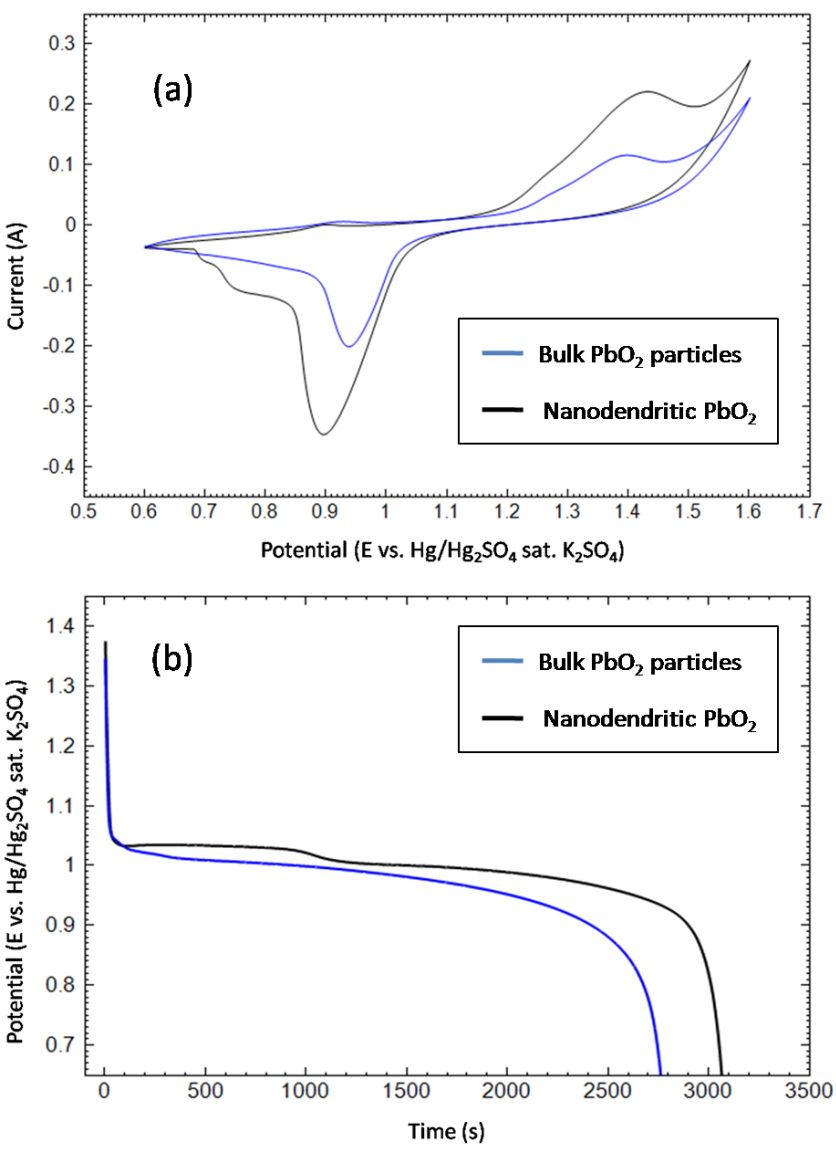

Figure 4.3: (a) Cyclic voltammetry at scanning rate of 10 mV/s and (b) first discharge capacity curves of nanodendritic and bulk PbO_2 particles.

Other than that, the first discharge capacity of nanodendritic and bulk PbO_2 was evaluated. Figure 4.3b demonstrates the first discharge curves of nanodendritic PbO_2 and bulk PbO_2 particles at 200 mAg^{-1} and cut-off voltage of 0.65 V (VS. Hg/Hg_2SO_4 sat.

K_2SO_4) in 4.7 M H_2SO_4. As 50 mg of active mixture was initially applied for both samples respectively to form PAM, the first discharge capacity figure of nanodendritic PbO_2 shows that the acquired capacity is 170 $mAhg^{-1}$, while bulk PbO_2 particles is 153 $mAhg^{-1}$. As compared to most of the researches conducted on nanostructured PbO_2 which are relatively low in initial discharge capacity [23], the nanodendritic PbO_2 in this experiment demonstrated higher initial discharge capacity even discharged at 200mAg^{-1}. Furthermore, higher discharge plateau is also observed in nanodendritic PbO_2 as compared to bulk PbO_2 particles.

4.4 Electrochemical property of as-synthesized nanostructured PbO in 12V automotive batteries

Table 4.1 summarizes the test results of C20 and CCA ratings being conducted.

Table 4.1: Test Results of C20 and CCA Ratings.

No.	Category	Sample 1 (Raw Battery Sample)	Sample 2	Sample 3	Sample 4	Sample 5
1	Label	NS60	40B24-N20	40B24-N100	40B24-P50	40B24-P100
2	Battery Model (Nominal Capacity)	40B24-9plates (35 Ah)	40B24-9plates (35 Ah)	40B24-9plates (35 Ah)	40B24-9plates (35 Ah)	40B24-9plates (35 Ah)
3	Positive Plate Characteristics	Conventional Plate (Ball Mill Oxide)	Conventional Plate (Ball Mill Oxide)	Conventional Plate (Ball Mill Oxide)	50% Nano PbO + 50% Ball Mill Oxide	100% Nano PbO
4	Negative Plate Characteristics	Conventional Plate (Ball Mill Oxide)	20% Nano PbO + 80% Ball Mill Oxide	100% Nano PbO	Conventional Plate (Ball Mill Oxide)	Conventional Plate (Ball Mill Oxide)

5	Open circuit CCA (Cold Cranking Ampere) after formation (after one-day rest and acid top-up)		350	380	385	396	375
6	1st C20 (Ah) Spec. ≥ 90% of Nominal Capacity		33.50	36.00	30.00	33.00	29.70
7	2nd C20 (Ah) Spec. ≥ 90% of Nominal Capacity		35.50	37.00	34.80	35.50	31.20
8	3rd C20 (Ah) Spec. ≥ 100% of Nominal Capacity		36.50	38.50	35.05	36.00	30.50
9	Voltage after 3rd C20 (V) Spec. = 12.70V ± 0.10V		12.70	12.75	12.70	12.77	This sample specification failed to achieve 100% C20 after 3rd cycle, therefore, no further test was conducted in commercial scale.
10	Acid SG after 3rd C20 Spec. = 1.27 ± 0.01 SG		1.28	1.28	1.28	1.28	
11	Open circuit CCA after 3rd C20 (By Midtronic Tester)		365	387	360	384	
12	CCA Test at -18 °C	1st Discharge Current (A)	270	270	270	270	
		Voltage at 30s (At least ≥ 7.2V)	7.5	7.78	6.05	8.02	
		2nd Discharge Current (A)	162	162	162	162	
		Duration at cut-off 6V after 2nd discharge current (At least ≥ 40 Second)	51.0	73.7	41.8	109.0	

According to the C20 results in Table 4.1, Sample 1 was the raw sample of typical commercial battery using only the conventional plates which had achieved the required capacity rating of 35.5 Ah than the nominal specification of 35 Ah in the second cycle of C20. Sample 2, with 20% of as-synthesized nanostructured PbO being used as the replacement into the raw material of negative plates, displayed the highest capacity rating among other battery samples across all cycles (36.0 Ah for the 1st C20, 37.0 Ah for the 2nd, and 38.5 Ah for the 3rd). Besides that, Sample 3, with 100% of as-synthesized nanostructured PbO being used as the raw material of negative plates, had shown among the lowest initial capacity rating of 30.0 Ah during the first cycle while slowly achieving the nominal specification in the 3rd C20 where 35.05 Ah was recorded. Subsequently, Sample 4, with 50% of as-synthesized nanostructured PbO being used as the replacement into raw material of positive plates, had indicated comparable capacity ratings with those of Sample 1, where 33.0 Ah was measured for the 1st C20, 35.5 Ah for the 2nd and 36.0 Ah for the 3rd.

However, Sample 5, with 100% of as-synthesized nanostructured PbO being used as the raw material of positive plates, had failed to achieve the nominal specification of capacity rating even after the 3rd C20, where 30.5 Ah was measured. Even though the surface area of the precursor used in positive plate is one of the determining factors in capacity rating, pore radius of inter-particles and the effective contact area between the current collector and also the active material, are also greatly important. With smaller pore radius in between the active material and fixed contact area of lead grid as the current collector, this might have limited the acid diffusion into the inner part of lead

plate for faradaic reaction, which leads to lower initial capacity rating as observed in Sample 5 [34-36].

On the other hand, Samples 1, 2, 3, and 4 which had passed the capacity rating test, were reconditioned to full state-of-charge for CCA tests at -18 ^{o}C. As can be seen in Table 4.1, Sample 4 had shown the highest final duration, 109 second after 2nd discharge (best CCA reading), followed by Sample 2 (73.7 second), Sample 1 (51 second). Sample 3 which failed to achieve the minimum voltage at 30 second after the 1st discharge, although it managed to last for 41.8 second after 2nd discharge. Meanwhile, Sample 5 had been discarded for the test as it failed to meet the C20 requirement.

Thus, with 20% of as-synthesized nanostructured PbO used as part of the raw material for negative plates in this study has shown the highest capacity rating among all samples, while 50% of the as-synthesized material as part of the material used in the positive plates alone, has displayed the highest CCA rating across all samples. This is also indicating that there is an optimum performance from 0% to 100% addition of the as-synthesized material into each conventional plate depending on what performance rating that needs to be optimized especially in this lead-grid system of lead-acid battery.

However, when 100% of the as-synthesized nanostructured PbO was used in the negative plates, the CCA result was not achieving the nominal specification as comparable to its counterpart of positive plates (100% as-synthesized nanostructured PbO) which failed to meet the nominal specification of C20.

Therefore, the result may signify that the as-synthesized nanostructured PbO might be a more feasible precursor for thin film lead-acid batteries with better electrochemical performance where the effective contact area between the active material and current collector is much higher than that of lead-grid system for better charge transfer.

Refer figures in appendix (Figure A, Figure B, Figure C, Figure D, Figure E and Figure F) for more validation of CCA results obtained via High Rate Bitrode Discharger for Sample 2, 3, and 4 which could be retrieved at Yokohama Batteries Sdn. Bhd. The figures show the final voltage at 30 second after 1^{st} discharge and final duration after 2^{nd} discharge when reaching cut-off voltage of 6V.

Conclusion

In summary, the flower-like PbO consisted of three dimensional nanoflakes was successfully synthesized via a simple chemical synthesis method and used to form nanodendritic PbO_2 as PAM for LAESD via electrochemical oxidation at constant voltage in the presence of electrolyte. The improved results of CV and first discharge capacity of nanodendritic PbO_2 than those of bulk PbO_2 particles suggest that the formation of nanodendrites on the primary surface of agglomerated PbO_2 provides larger crystallite network structures for better material utilization at high discharge rate.

This work can help identify the essential unique morphology of starting precursor, where its crystals growth is dependent on discontinuous surface, can be used as a substrate to form nanodendritic material with better network structure via electrochemical oxidation at constant voltage for improving electrochemical performance of LAESD.

Preliminary results of the material tested in 12V automotive batteries show that it could be a promising electrode material for producing commercial LAESD especially the new generation of thin film lead-acid batteries.

Future Planning

The success of this preliminary work in identifying potential electrochemical performance attributed to the unique morphology of the as-synthesized material used as the starting precursor for lead-acid cell has unraveled immense future opportunities and efforts needed to fulfill the global objective in producing a prototype of lead-acid hybrid supercapacitor.

Based on the results in this work, future research will emphasize on the following categories:

- The as-synthesized material to be tested in thin film lead-acid batteries.
- The material synthesis method to be extended into producing lead oxide nanoparticles by using recycled scrap lead paste as raw material to meet objective cost and scalable production feasibility.
- Identifying a common reducing or oxidizing solvent to be applied in the synthesis process to produce lead(II) or lead(IV) oxide nanoparticles with better cycling life.
- Constructing a prototype of lead-acid hybrid supercapacitor with the as-synthesized materials in both electrodes for evaluation.

REFERENCES

1. DAJ Rand, PT Moseley. 2009. Secondary Batteries - Lead-Acid System. Elsevier.
2. DAJ Rand, PT Moseley, J Garche, CD Parker. 2004. Valve-regulated Lead-Acid Batteries. Elsevier.
3. Koichi Fukuo, Akira Fujimura, Masaaki Saito, Kazuhiko Tsunoda, Shiro Takiguchi. JSAE Review 2001;22:95-103.
4. Siang Fui Tie, Chee Wei Tan. Renewable and Sustainable Energy Review 2013;20:82-102.
5. Ting Chen, Houyi Ma, Delong Kong. Material Letters 2013;90:103-106.
6. Nengfei Yu, Lijun Gao. Electrochemistry Communications 2009;11:220-222.
7. AJ Fairweather, DA Stone, MP Foster. Journal of Power Sources 2013;226:191-201.
8. Yang M. Journal of Material Chemistry 2011;21:3119–24.
9. M Cruz, L Hernan, J Morales, L Sanchez. Journal of Power Sources 2002;108:35.
10. DL Perry, TJ Wilkinson. Appl. Phys. A-Mat. Sci. Pro. 2007;89:77-80.
11. B Jia, L Gao. Material Chemistry and Physics 2006;100:351-354.
12. Karami Hasan, Karimi Mohammad Ali, Haghdar Saeed, Sadeghi Abbas, Mir-Ghasemi Rasool, Mahdi-Khani Saeed. Material Chemistry and Physics 2008;108:337-44.
13. Sajjad Damiri, Hassan Yousofian Varzaneh, Hamid Reza Ebrahimi. Materials Letters 2011;65:2598-2600.

14. Chen Ting, Huang Hui, Ma Houyi, Kong Delong. Electrochimica Acta 2013;88:79-85.
15. Y Zhang, Y Liu, M Liu, Chem. Mater. 2006;18:4643-4646.
16. Pollet Bruno G, Staffell Iain, Shang Jin Lei. Electrochimica Acta 2012;84:235-49.
17. PT Moseley, DAJ Rand, Monahov Boris. Journal of Power Sources 2012;219:79-9.
18. TL Blair. Journal of Power Sources 1998;73:47-55.
19. Pradyot Patnaik. 2003. Handbook of Inorganic Chemicals. McGraw-Hill.
20. K Konstantinov, SH Ng, JZ Wang, GX Wang, D Wxler, HK Liu. Journal of Power Sources 2007;159:241.
21. H Karami, MA Karimi, S Haghdar. Materials Research Bulletin 2008;43:3054-3065.
22. JH Zhang, XG Yang, DW Wang, Y Xie, YT Qian. Inorganic Chemistry Communication 1999;2:447.
23. Gao Pengran, Liu Yi, Bu Xianfu, Hu Meng, Dai Yuan, Gao Xiaorui. Journal of Power Sources 2013;242:299-304.
24. Kwestroo W, Huizing. A. J lnorg Nucl Chem 1965;27:1951-4.
25. Vere AW. 1987. Crystal growth: principles and progress. New York: Plenum.
26. GZ Cao. 2004. Nanostructures and nanomaterials: synthesis, properties and applications. London: Imperial College Press.
27. Witten TA, Sander LM. Phys Rev Lett 1981;47:1400-3.
28. Visscher W. Journal of Power Sources 1977;1:257–66.

29. Ding Liang-Xin, Zheng Fu-Lin,Wang Jian-Wei, Li Gao-Ren, Wang Zi-Long, Tong Ye-Xiang. Chemistry Communications 2012; 48:1275–7.
30. Eric J. Mittemeijer, Udo Wezel. 2013. Modern Diffraction Methods. Wiley-VCH.
31. Yang Leng. 2013. Materials Characterization: Introduction to Microscopic and Spectroscopic Methods. Wiley-VCH.
32. S.M. Khopkar. 2012. Basic Concept of Analytical Chemistry. New Academic Science.
33. JIS D 5301. 2006. Japanese Industrial Standard for Lead-acid Starter Batteries.
34. E.E. Ferg, P. Loyson, N. Rust. Journal of Power Sources 2005;141:316-325.
35. J. Garche. Journal of Power Sources 1990;30:47-54.
36. Yonglang Guo, Mengdeng Wu, Shounan Hua. Journal of Power Sources 1997;64:65-69.

APPENDIX

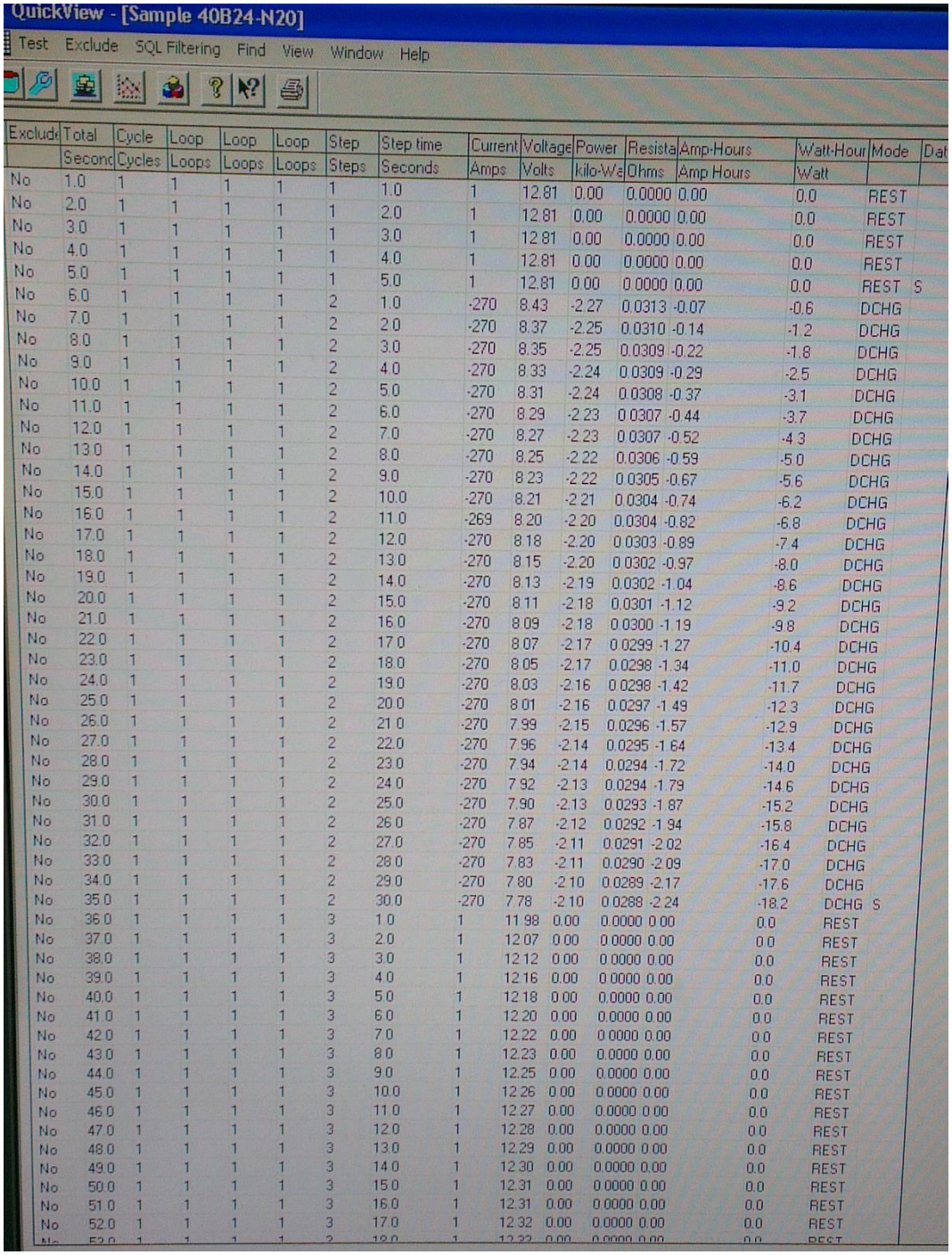

QuickView - [Sample 40B24-N20]

Test Exclude SQL Filtering Find View Window Help

Exclude	Total Seconds	Cycle Cycles	Loop Loops	Loop Loops	Loop Loops	Step Steps	Step time Seconds	Current Amps	Voltage Volts	Power kilo-Wa	Resista Ohms	Amp-Hours Amp Hours	Watt-Hour Watt	Mode	Dat
No	1.0	1	1	1	1	1	1.0	1	12.81	0.00	0.0000	0.00	0.0	REST	
No	2.0	1	1	1	1	1	2.0	1	12.81	0.00	0.0000	0.00	0.0	REST	
No	3.0	1	1	1	1	1	3.0	1	12.81	0.00	0.0000	0.00	0.0	REST	
No	4.0	1	1	1	1	1	4.0	1	12.81	0.00	0.0000	0.00	0.0	REST	
No	5.0	1	1	1	1	1	5.0	1	12.81	0.00	0.0000	0.00	0.0	REST	S
No	6.0	1	1	1	1	2	1.0	-270	8.43	-2.27	0.0313	-0.07	-0.6	DCHG	
No	7.0	1	1	1	1	2	2.0	-270	8.37	-2.25	0.0310	-0.14	-1.2	DCHG	
No	8.0	1	1	1	1	2	3.0	-270	8.35	-2.25	0.0309	-0.22	-1.8	DCHG	
No	9.0	1	1	1	1	2	4.0	-270	8.33	-2.24	0.0309	-0.29	-2.5	DCHG	
No	10.0	1	1	1	1	2	5.0	-270	8.31	-2.24	0.0308	-0.37	-3.1	DCHG	
No	11.0	1	1	1	1	2	6.0	-270	8.29	-2.23	0.0307	-0.44	-3.7	DCHG	
No	12.0	1	1	1	1	2	7.0	-270	8.27	-2.23	0.0307	-0.52	-4.3	DCHG	
No	13.0	1	1	1	1	2	8.0	-270	8.25	-2.22	0.0306	-0.59	-5.0	DCHG	
No	14.0	1	1	1	1	2	9.0	-270	8.23	-2.22	0.0305	-0.67	-5.6	DCHG	
No	15.0	1	1	1	1	2	10.0	-270	8.21	-2.21	0.0304	-0.74	-6.2	DCHG	
No	16.0	1	1	1	1	2	11.0	-269	8.20	-2.20	0.0304	-0.82	-6.8	DCHG	
No	17.0	1	1	1	1	2	12.0	-270	8.18	-2.20	0.0303	-0.89	-7.4	DCHG	
No	18.0	1	1	1	1	2	13.0	-270	8.15	-2.20	0.0302	-0.97	-8.0	DCHG	
No	19.0	1	1	1	1	2	14.0	-270	8.13	-2.19	0.0302	-1.04	-8.6	DCHG	
No	20.0	1	1	1	1	2	15.0	-270	8.11	-2.18	0.0301	-1.12	-9.2	DCHG	
No	21.0	1	1	1	1	2	16.0	-270	8.09	-2.18	0.0300	-1.19	-9.8	DCHG	
No	22.0	1	1	1	1	2	17.0	-270	8.07	-2.17	0.0299	-1.27	-10.4	DCHG	
No	23.0	1	1	1	1	2	18.0	-270	8.05	-2.17	0.0298	-1.34	-11.0	DCHG	
No	24.0	1	1	1	1	2	19.0	-270	8.03	-2.16	0.0298	-1.42	-11.7	DCHG	
No	25.0	1	1	1	1	2	20.0	-270	8.01	-2.16	0.0297	-1.49	-12.3	DCHG	
No	26.0	1	1	1	1	2	21.0	-270	7.99	-2.15	0.0296	-1.57	-12.9	DCHG	
No	27.0	1	1	1	1	2	22.0	-270	7.96	-2.14	0.0295	-1.64	-13.4	DCHG	
No	28.0	1	1	1	1	2	23.0	-270	7.94	-2.14	0.0294	-1.72	-14.0	DCHG	
No	29.0	1	1	1	1	2	24.0	-270	7.92	-2.13	0.0294	-1.79	-14.6	DCHG	
No	30.0	1	1	1	1	2	25.0	-270	7.90	-2.13	0.0293	-1.87	-15.2	DCHG	
No	31.0	1	1	1	1	2	26.0	-270	7.87	-2.12	0.0292	-1.94	-15.8	DCHG	
No	32.0	1	1	1	1	2	27.0	-270	7.85	-2.11	0.0291	-2.02	-16.4	DCHG	
No	33.0	1	1	1	1	2	28.0	-270	7.83	-2.11	0.0290	-2.09	-17.0	DCHG	
No	34.0	1	1	1	1	2	29.0	-270	7.80	-2.10	0.0289	-2.17	-17.6	DCHG	
No	35.0	1	1	1	1	2	30.0	-270	7.78	-2.10	0.0288	-2.24	-18.2	DCHG	S
No	36.0	1	1	1	1	3	1.0	1	11.98	0.00	0.0000	0.00	0.0	REST	
No	37.0	1	1	1	1	3	2.0	1	12.07	0.00	0.0000	0.00	0.0	REST	
No	38.0	1	1	1	1	3	3.0	1	12.12	0.00	0.0000	0.00	0.0	REST	
No	39.0	1	1	1	1	3	4.0	1	12.16	0.00	0.0000	0.00	0.0	REST	
No	40.0	1	1	1	1	3	5.0	1	12.18	0.00	0.0000	0.00	0.0	REST	
No	41.0	1	1	1	1	3	6.0	1	12.20	0.00	0.0000	0.00	0.0	REST	
No	42.0	1	1	1	1	3	7.0	1	12.22	0.00	0.0000	0.00	0.0	REST	
No	43.0	1	1	1	1	3	8.0	1	12.23	0.00	0.0000	0.00	0.0	REST	
No	44.0	1	1	1	1	3	9.0	1	12.25	0.00	0.0000	0.00	0.0	REST	
No	45.0	1	1	1	1	3	10.0	1	12.26	0.00	0.0000	0.00	0.0	REST	
No	46.0	1	1	1	1	3	11.0	1	12.27	0.00	0.0000	0.00	0.0	REST	
No	47.0	1	1	1	1	3	12.0	1	12.28	0.00	0.0000	0.00	0.0	REST	
No	48.0	1	1	1	1	3	13.0	1	12.29	0.00	0.0000	0.00	0.0	REST	
No	49.0	1	1	1	1	3	14.0	1	12.30	0.00	0.0000	0.00	0.0	REST	
No	50.0	1	1	1	1	3	15.0	1	12.31	0.00	0.0000	0.00	0.0	REST	
No	51.0	1	1	1	1	3	16.0	1	12.31	0.00	0.0000	0.00	0.0	REST	
No	52.0	1	1	1	1	3	17.0	1	12.32	0.00	0.0000	0.00	0.0	REST	

Figure A: Battery Sample 2 (40B24-N20), final voltage at 30s during 1st discharge of CCA rating.

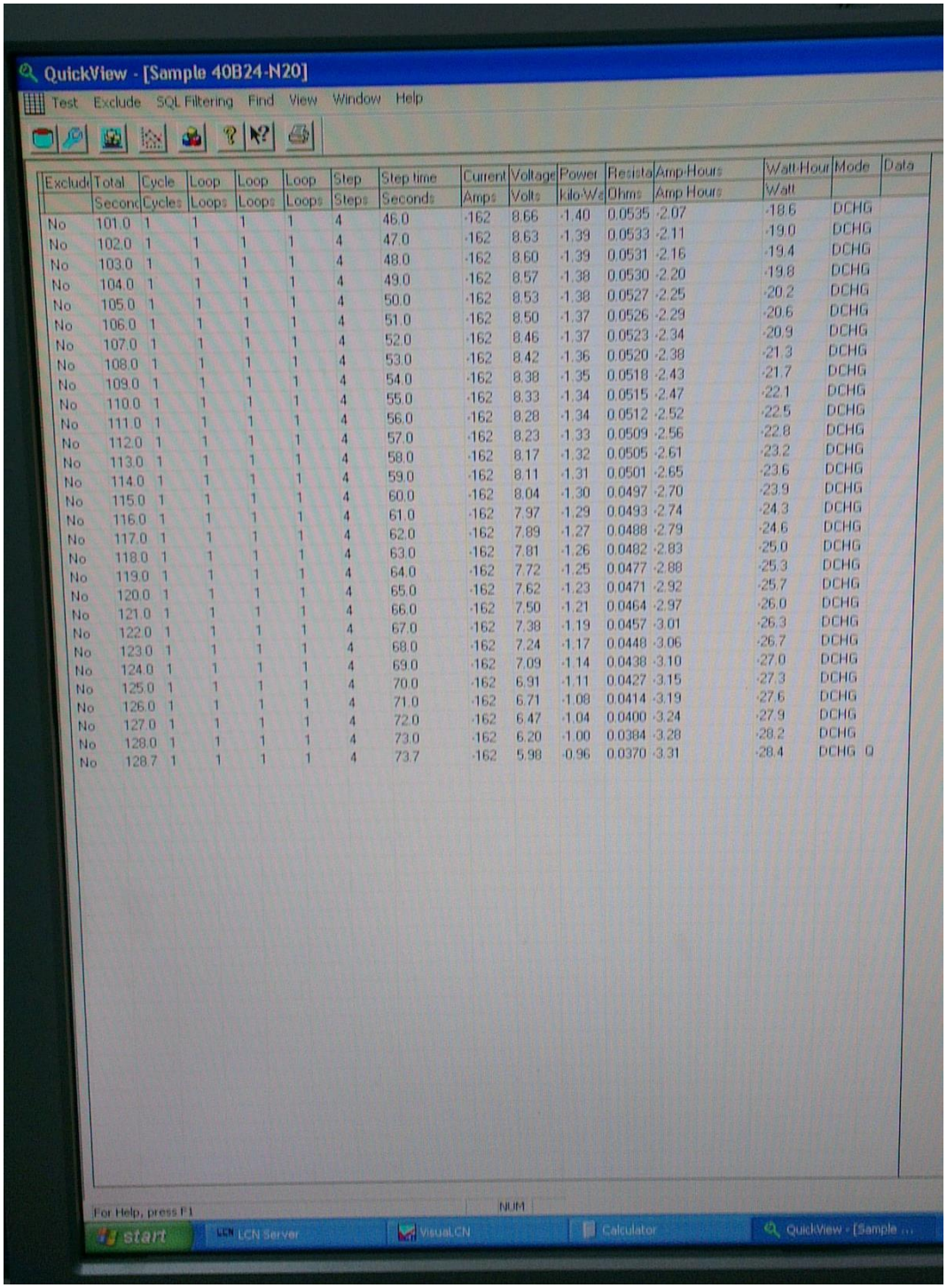

Exclude	Total Seconds	Cycle Cycles	Loop Loops	Loop Loops	Loop Loops	Step Steps	Step time Seconds	Current Amps	Voltage Volts	Power kilo-Wa	Resista Ohms	Amp-Hours Amp-Hours	Watt-Hour Watt	Mode	Data
No	101.0	1	1	1	1	4	46.0	-162	8.66	-1.40	0.0535	-2.07	-18.6	DCHG	
No	102.0	1	1	1	1	4	47.0	-162	8.63	-1.39	0.0533	-2.11	-19.0	DCHG	
No	103.0	1	1	1	1	4	48.0	-162	8.60	-1.39	0.0531	-2.16	-19.4	DCHG	
No	104.0	1	1	1	1	4	49.0	-162	8.57	-1.38	0.0530	-2.20	-19.8	DCHG	
No	105.0	1	1	1	1	4	50.0	-162	8.53	-1.38	0.0527	-2.25	-20.2	DCHG	
No	106.0	1	1	1	1	4	51.0	-162	8.50	-1.37	0.0526	-2.29	-20.6	DCHG	
No	107.0	1	1	1	1	4	52.0	-162	8.46	-1.37	0.0523	-2.34	-20.9	DCHG	
No	108.0	1	1	1	1	4	53.0	-162	8.42	-1.36	0.0520	-2.38	-21.3	DCHG	
No	109.0	1	1	1	1	4	54.0	-162	8.38	-1.35	0.0518	-2.43	-21.7	DCHG	
No	110.0	1	1	1	1	4	55.0	-162	8.33	-1.34	0.0515	-2.47	-22.1	DCHG	
No	111.0	1	1	1	1	4	56.0	-162	8.28	-1.34	0.0512	-2.52	-22.5	DCHG	
No	112.0	1	1	1	1	4	57.0	-162	8.23	-1.33	0.0509	-2.56	-22.8	DCHG	
No	113.0	1	1	1	1	4	58.0	-162	8.17	-1.32	0.0505	-2.61	-23.2	DCHG	
No	114.0	1	1	1	1	4	59.0	-162	8.11	-1.31	0.0501	-2.65	-23.6	DCHG	
No	115.0	1	1	1	1	4	60.0	-162	8.04	-1.30	0.0497	-2.70	-23.9	DCHG	
No	116.0	1	1	1	1	4	61.0	-162	7.97	-1.29	0.0493	-2.74	-24.3	DCHG	
No	117.0	1	1	1	1	4	62.0	-162	7.89	-1.27	0.0488	-2.79	-24.6	DCHG	
No	118.0	1	1	1	1	4	63.0	-162	7.81	-1.26	0.0482	-2.83	-25.0	DCHG	
No	119.0	1	1	1	1	4	64.0	-162	7.72	-1.25	0.0477	-2.88	-25.3	DCHG	
No	120.0	1	1	1	1	4	65.0	-162	7.62	-1.23	0.0471	-2.92	-25.7	DCHG	
No	121.0	1	1	1	1	4	66.0	-162	7.50	-1.21	0.0464	-2.97	-26.0	DCHG	
No	122.0	1	1	1	1	4	67.0	-162	7.38	-1.19	0.0457	-3.01	-26.3	DCHG	
No	123.0	1	1	1	1	4	68.0	-162	7.24	-1.17	0.0448	-3.06	-26.7	DCHG	
No	124.0	1	1	1	1	4	69.0	-162	7.09	-1.14	0.0438	-3.10	-27.0	DCHG	
No	125.0	1	1	1	1	4	70.0	-162	6.91	-1.11	0.0427	-3.15	-27.3	DCHG	
No	126.0	1	1	1	1	4	71.0	-162	6.71	-1.08	0.0414	-3.19	-27.6	DCHG	
No	127.0	1	1	1	1	4	72.0	-162	6.47	-1.04	0.0400	-3.24	-27.9	DCHG	
No	128.0	1	1	1	1	4	73.0	-162	6.20	-1.00	0.0384	-3.28	-28.2	DCHG	
No	128.7	1	1	1	1	4	73.7	-162	5.98	-0.96	0.0370	-3.31	-28.4	DCHG	Q

Figure B: Battery Sample 2 (40B24-N20), final duration during 2nd discharge of CCA rating.

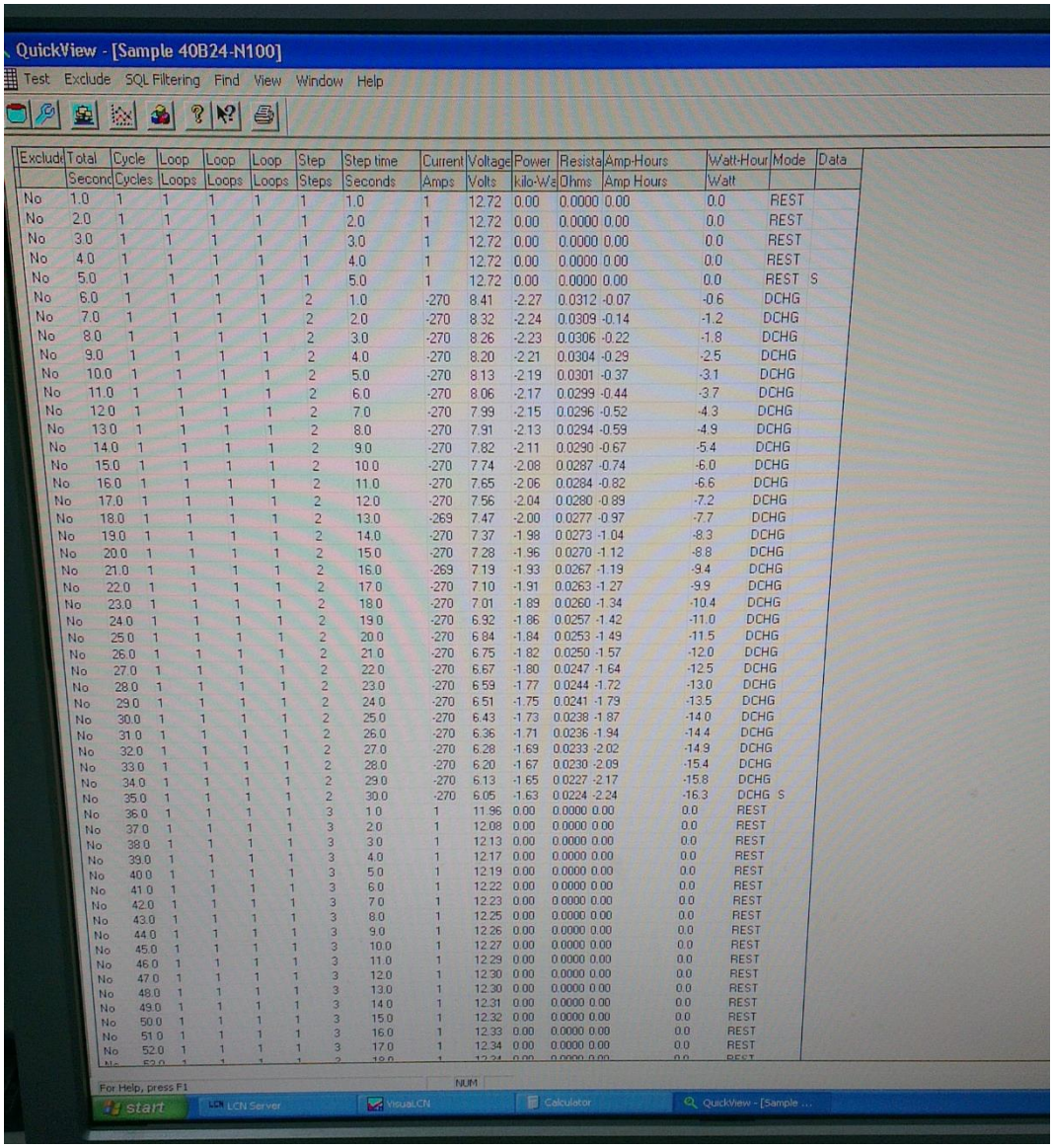

Exclude	Total Seconds	Cycle Cycles	Loop Loops	Loop Loops	Loop Loops	Step Steps	Step time Seconds	Current Amps	Voltage Volts	Power kilo-Wa	Resista Ohms	Amp-Hours Amp Hours	Watt-Hour Watt	Mode	Data
No	1.0	1	1	1	1	1	1.0	1	12.72	0.00	0.0000	0.00	0.0	REST	
No	2.0	1	1	1	1	1	2.0	1	12.72	0.00	0.0000	0.00	0.0	REST	
No	3.0	1	1	1	1	1	3.0	1	12.72	0.00	0.0000	0.00	0.0	REST	
No	4.0	1	1	1	1	1	4.0	1	12.72	0.00	0.0000	0.00	0.0	REST	
No	5.0	1	1	1	1	1	5.0	1	12.72	0.00	0.0000	0.00	0.0	REST	S
No	6.0	1	1	1	1	2	1.0	-270	8.41	-2.27	0.0312	-0.07	-0.6	DCHG	
No	7.0	1	1	1	1	2	2.0	-270	8.32	-2.24	0.0309	-0.14	-1.2	DCHG	
No	8.0	1	1	1	1	2	3.0	-270	8.26	-2.23	0.0306	-0.22	-1.8	DCHG	
No	9.0	1	1	1	1	2	4.0	-270	8.20	-2.21	0.0304	-0.29	-2.5	DCHG	
No	10.0	1	1	1	1	2	5.0	-270	8.13	-2.19	0.0301	-0.37	-3.1	DCHG	
No	11.0	1	1	1	1	2	6.0	-270	8.06	-2.17	0.0299	-0.44	-3.7	DCHG	
No	12.0	1	1	1	1	2	7.0	-270	7.99	-2.15	0.0296	-0.52	-4.3	DCHG	
No	13.0	1	1	1	1	2	8.0	-270	7.91	-2.13	0.0294	-0.59	-4.9	DCHG	
No	14.0	1	1	1	1	2	9.0	-270	7.82	-2.11	0.0290	-0.67	-5.4	DCHG	
No	15.0	1	1	1	1	2	10.0	-270	7.74	-2.08	0.0287	-0.74	-6.0	DCHG	
No	16.0	1	1	1	1	2	11.0	-270	7.65	-2.06	0.0284	-0.82	-6.6	DCHG	
No	17.0	1	1	1	1	2	12.0	-270	7.56	-2.04	0.0280	-0.89	-7.2	DCHG	
No	18.0	1	1	1	1	2	13.0	-269	7.47	-2.00	0.0277	-0.97	-7.7	DCHG	
No	19.0	1	1	1	1	2	14.0	-270	7.37	-1.98	0.0273	-1.04	-8.3	DCHG	
No	20.0	1	1	1	1	2	15.0	-270	7.28	-1.96	0.0270	-1.12	-8.8	DCHG	
No	21.0	1	1	1	1	2	16.0	-269	7.19	-1.93	0.0267	-1.19	-9.4	DCHG	
No	22.0	1	1	1	1	2	17.0	-270	7.10	-1.91	0.0263	-1.27	-9.9	DCHG	
No	23.0	1	1	1	1	2	18.0	-270	7.01	-1.89	0.0260	-1.34	-10.4	DCHG	
No	24.0	1	1	1	1	2	19.0	-270	6.92	-1.86	0.0257	-1.42	-11.0	DCHG	
No	25.0	1	1	1	1	2	20.0	-270	6.84	-1.84	0.0253	-1.49	-11.5	DCHG	
No	26.0	1	1	1	1	2	21.0	-270	6.75	-1.82	0.0250	-1.57	-12.0	DCHG	
No	27.0	1	1	1	1	2	22.0	-270	6.67	-1.80	0.0247	-1.64	-12.5	DCHG	
No	28.0	1	1	1	1	2	23.0	-270	6.59	-1.77	0.0244	-1.72	-13.0	DCHG	
No	29.0	1	1	1	1	2	24.0	-270	6.51	-1.75	0.0241	-1.79	-13.5	DCHG	
No	30.0	1	1	1	1	2	25.0	-270	6.43	-1.73	0.0238	-1.87	-14.0	DCHG	
No	31.0	1	1	1	1	2	26.0	-270	6.36	-1.71	0.0236	-1.94	-14.4	DCHG	
No	32.0	1	1	1	1	2	27.0	-270	6.28	-1.69	0.0233	-2.02	-14.9	DCHG	
No	33.0	1	1	1	1	2	28.0	-270	6.20	-1.67	0.0230	-2.09	-15.4	DCHG	
No	34.0	1	1	1	1	2	29.0	-270	6.13	-1.65	0.0227	-2.17	-15.8	DCHG	
No	35.0	1	1	1	1	2	30.0	-270	6.05	-1.63	0.0224	-2.24	-16.3	DCHG	S
No	36.0	1	1	1	1	3	1.0	1	11.96	0.00	0.0000	0.00	0.0	REST	
No	37.0	1	1	1	1	3	2.0	1	12.08	0.00	0.0000	0.00	0.0	REST	
No	38.0	1	1	1	1	3	3.0	1	12.13	0.00	0.0000	0.00	0.0	REST	
No	39.0	1	1	1	1	3	4.0	1	12.17	0.00	0.0000	0.00	0.0	REST	
No	40.0	1	1	1	1	3	5.0	1	12.19	0.00	0.0000	0.00	0.0	REST	
No	41.0	1	1	1	1	3	6.0	1	12.22	0.00	0.0000	0.00	0.0	REST	
No	42.0	1	1	1	1	3	7.0	1	12.23	0.00	0.0000	0.00	0.0	REST	
No	43.0	1	1	1	1	3	8.0	1	12.25	0.00	0.0000	0.00	0.0	REST	
No	44.0	1	1	1	1	3	9.0	1	12.26	0.00	0.0000	0.00	0.0	REST	
No	45.0	1	1	1	1	3	10.0	1	12.27	0.00	0.0000	0.00	0.0	REST	
No	46.0	1	1	1	1	3	11.0	1	12.29	0.00	0.0000	0.00	0.0	REST	
No	47.0	1	1	1	1	3	12.0	1	12.30	0.00	0.0000	0.00	0.0	REST	
No	48.0	1	1	1	1	3	13.0	1	12.30	0.00	0.0000	0.00	0.0	REST	
No	49.0	1	1	1	1	3	14.0	1	12.31	0.00	0.0000	0.00	0.0	REST	
No	50.0	1	1	1	1	3	15.0	1	12.32	0.00	0.0000	0.00	0.0	REST	
No	51.0	1	1	1	1	3	16.0	1	12.33	0.00	0.0000	0.00	0.0	REST	
No	52.0	1	1	1	1	3	17.0	1	12.34	0.00	0.0000	0.00	0.0	REST	

Figure C: Battery Sample 3 (40B24-N100), final voltage at 30s during 1st discharge of CCA rating.

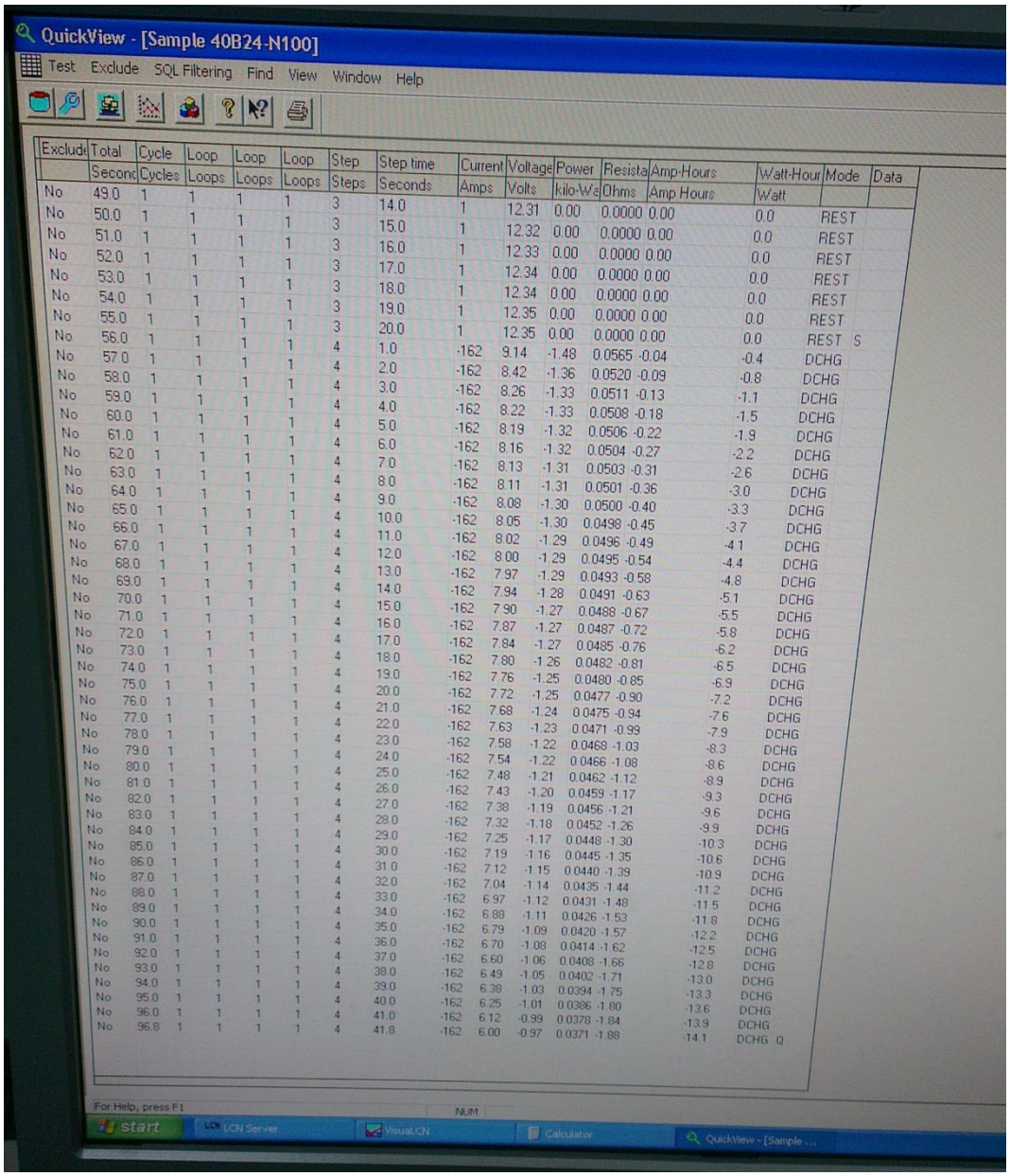

Exclude	Total Seconds	Cycle Cycles	Loop Loops	Loop Loops	Loop Loops	Step Steps	Step time Seconds	Current Amps	Voltage Volts	Power kilo-Wa	Resista Ohms	Amp-Hours Amp Hours	Watt-Hour Watt	Mode	Data
No	49.0	1	1	1	1	3	14.0	1	12.31	0.00	0.0000	0.00	0.0	REST	
No	50.0	1	1	1	1	3	15.0	1	12.32	0.00	0.0000	0.00	0.0	REST	
No	51.0	1	1	1	1	3	16.0	1	12.33	0.00	0.0000	0.00	0.0	REST	
No	52.0	1	1	1	1	3	17.0	1	12.34	0.00	0.0000	0.00	0.0	REST	
No	53.0	1	1	1	1	3	18.0	1	12.34	0.00	0.0000	0.00	0.0	REST	
No	54.0	1	1	1	1	3	19.0	1	12.35	0.00	0.0000	0.00	0.0	REST	
No	55.0	1	1	1	1	3	20.0	1	12.35	0.00	0.0000	0.00	0.0	REST	
No	56.0	1	1	1	1	4	1.0	-162	9.14	-1.48	0.0565	-0.04	-0.4	DCHG	
No	57.0	1	1	1	1	4	2.0	-162	8.42	-1.36	0.0520	-0.09	-0.8	DCHG	
No	58.0	1	1	1	1	4	3.0	-162	8.26	-1.33	0.0511	-0.13	-1.1	DCHG	
No	59.0	1	1	1	1	4	4.0	-162	8.22	-1.33	0.0508	-0.18	-1.5	DCHG	
No	60.0	1	1	1	1	4	5.0	-162	8.19	-1.32	0.0506	-0.22	-1.9	DCHG	
No	61.0	1	1	1	1	4	6.0	-162	8.16	-1.32	0.0504	-0.27	-2.2	DCHG	
No	62.0	1	1	1	1	4	7.0	-162	8.13	-1.31	0.0503	-0.31	-2.6	DCHG	
No	63.0	1	1	1	1	4	8.0	-162	8.11	-1.31	0.0501	-0.36	-3.0	DCHG	
No	64.0	1	1	1	1	4	9.0	-162	8.08	-1.30	0.0500	-0.40	-3.3	DCHG	
No	65.0	1	1	1	1	4	10.0	-162	8.05	-1.30	0.0498	-0.45	-3.7	DCHG	
No	66.0	1	1	1	1	4	11.0	-162	8.02	-1.29	0.0496	-0.49	-4.1	DCHG	
No	67.0	1	1	1	1	4	12.0	-162	8.00	-1.29	0.0495	-0.54	-4.4	DCHG	
No	68.0	1	1	1	1	4	13.0	-162	7.97	-1.29	0.0493	-0.58	-4.8	DCHG	
No	69.0	1	1	1	1	4	14.0	-162	7.94	-1.28	0.0491	-0.63	-5.1	DCHG	
No	70.0	1	1	1	1	4	15.0	-162	7.90	-1.27	0.0488	-0.67	-5.5	DCHG	
No	71.0	1	1	1	1	4	16.0	-162	7.87	-1.27	0.0487	-0.72	-5.8	DCHG	
No	72.0	1	1	1	1	4	17.0	-162	7.84	-1.27	0.0485	-0.76	-6.2	DCHG	
No	73.0	1	1	1	1	4	18.0	-162	7.80	-1.26	0.0482	-0.81	-6.5	DCHG	
No	74.0	1	1	1	1	4	19.0	-162	7.76	-1.25	0.0480	-0.85	-6.9	DCHG	
No	75.0	1	1	1	1	4	20.0	-162	7.72	-1.25	0.0477	-0.90	-7.2	DCHG	
No	76.0	1	1	1	1	4	21.0	-162	7.68	-1.24	0.0475	-0.94	-7.6	DCHG	
No	77.0	1	1	1	1	4	22.0	-162	7.63	-1.23	0.0471	-0.99	-7.9	DCHG	
No	78.0	1	1	1	1	4	23.0	-162	7.58	-1.22	0.0468	-1.03	-8.3	DCHG	
No	79.0	1	1	1	1	4	24.0	-162	7.54	-1.22	0.0466	-1.08	-8.6	DCHG	
No	80.0	1	1	1	1	4	25.0	-162	7.48	-1.21	0.0462	-1.12	-8.9	DCHG	
No	81.0	1	1	1	1	4	26.0	-162	7.43	-1.20	0.0459	-1.17	-9.3	DCHG	
No	82.0	1	1	1	1	4	27.0	-162	7.38	-1.19	0.0456	-1.21	-9.6	DCHG	
No	83.0	1	1	1	1	4	28.0	-162	7.32	-1.18	0.0452	-1.26	-9.9	DCHG	
No	84.0	1	1	1	1	4	29.0	-162	7.25	-1.17	0.0448	-1.30	-10.3	DCHG	
No	85.0	1	1	1	1	4	30.0	-162	7.19	-1.16	0.0445	-1.35	-10.6	DCHG	
No	86.0	1	1	1	1	4	31.0	-162	7.12	-1.15	0.0440	-1.39	-10.9	DCHG	
No	87.0	1	1	1	1	4	32.0	-162	7.04	-1.14	0.0435	-1.44	-11.2	DCHG	
No	88.0	1	1	1	1	4	33.0	-162	6.97	-1.12	0.0431	-1.48	-11.5	DCHG	
No	89.0	1	1	1	1	4	34.0	-162	6.88	-1.11	0.0426	-1.53	-11.8	DCHG	
No	90.0	1	1	1	1	4	35.0	-162	6.79	-1.09	0.0420	-1.57	-12.2	DCHG	
No	91.0	1	1	1	1	4	36.0	-162	6.70	-1.08	0.0414	-1.62	-12.5	DCHG	
No	92.0	1	1	1	1	4	37.0	-162	6.60	-1.06	0.0408	-1.66	-12.8	DCHG	
No	93.0	1	1	1	1	4	38.0	-162	6.49	-1.05	0.0402	-1.71	-13.0	DCHG	
No	94.0	1	1	1	1	4	39.0	-162	6.38	-1.03	0.0394	-1.75	-13.3	DCHG	
No	95.0	1	1	1	1	4	40.0	-162	6.25	-1.01	0.0386	-1.80	-13.6	DCHG	
No	96.0	1	1	1	1	4	41.0	-162	6.12	-0.99	0.0378	-1.84	-13.9	DCHG	
No	96.8	1	1	1	1	4	41.8	-162	6.00	-0.97	0.0371	-1.88	-14.1	DCHG	0

Figure D: Battery Sample 3 (40B24-N100), final duration during 2nd discharge of CCA rating.

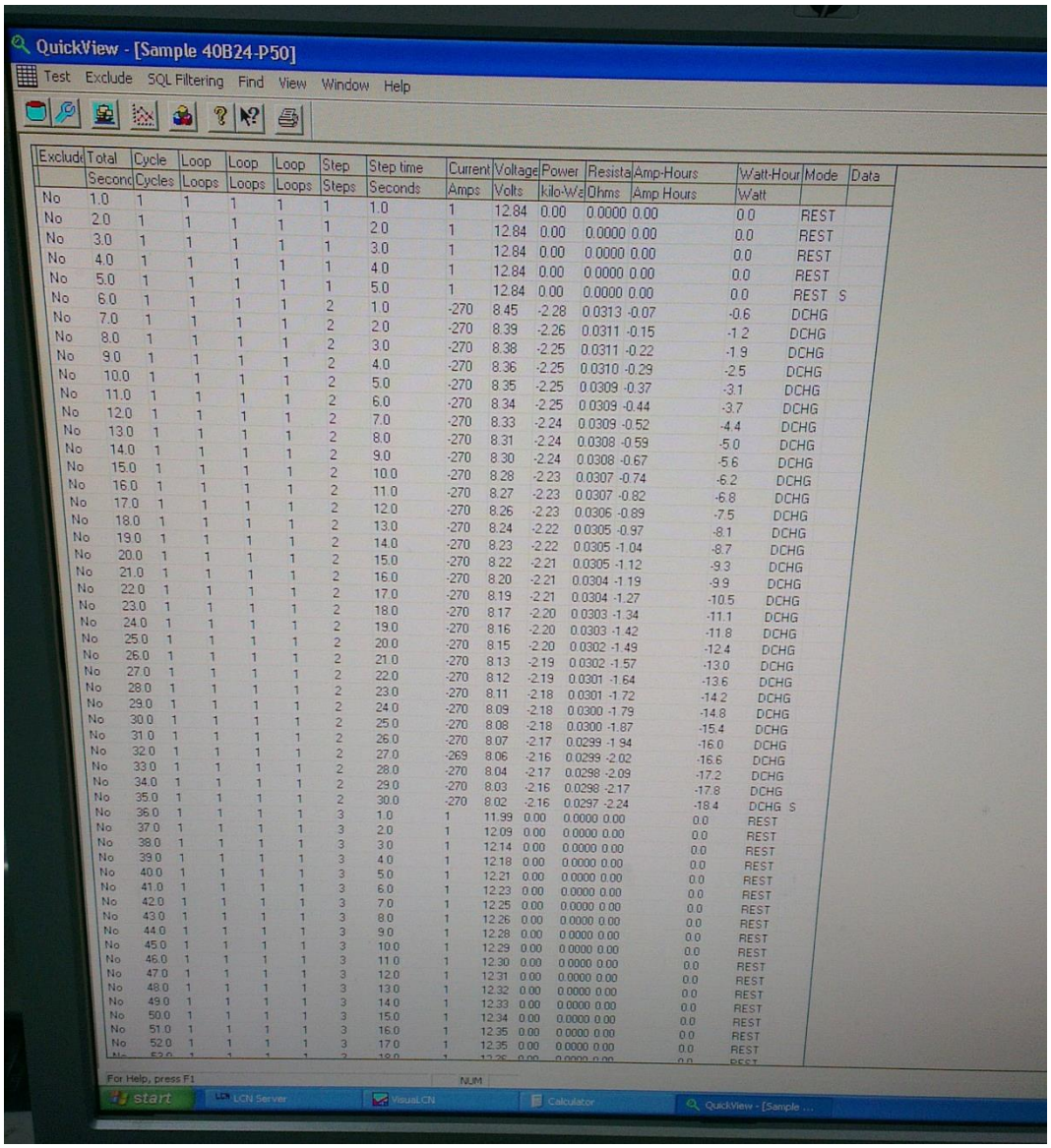

Figure E: Battery Sample 4 (40B24-P50), final voltage at 30s during 1st discharge of CCA rating.

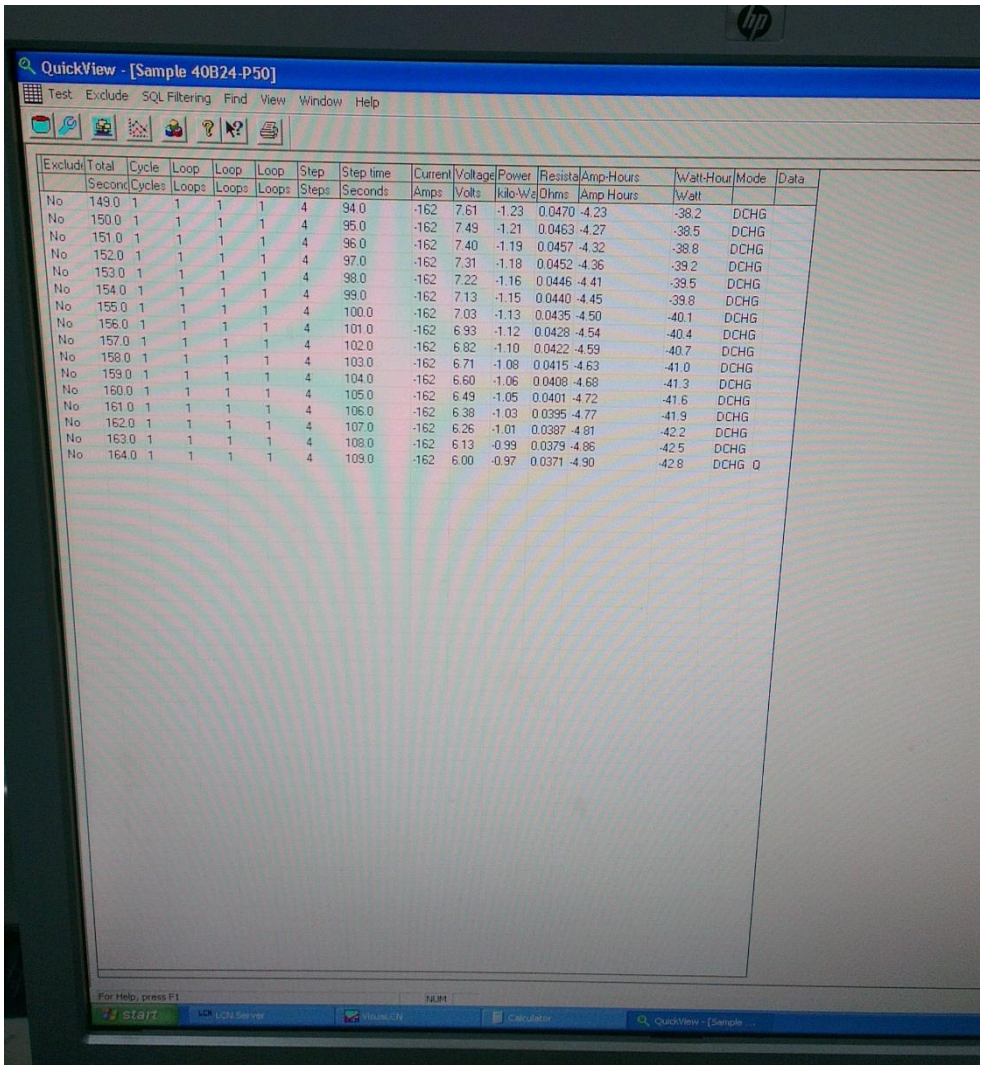

Figure F: Battery Sample 4 (40B24-P50), final duration during 2nd discharge of CCA rating.